AUTOPHAGY OF METALLOTHIONEINS PREVENTS TNF-INDUCED OXIDATIVE STRESS AND TOXICITY IN HEPATOMA CELLS

Ullio, Chiara; Brunk, Ulf T.; Urani, Chiara; Melchioretto, Pasquale; Bonelli, Gabriella; Baccino, Francesco M.; Autelli, Riccardo. AUTOPHAGY OF METALLOTHIONEINS PREVENTS TNF-INDUCED OXIDATIVE STRESS AND TOXICITY IN HEPATOMA CELLS. AUTOPHAGY. 11 (12) pp: 2184-2198.
DOI: 10.1080/15548627.2015.1106662

AUTOPHAGY OF METALLOTHIONEINS PREVENTS TNF-INDUCED OXIDATIVE STRESS AND TOXICITY IN HEPATOMA CELLS

Chiara Ullio[1], Ulf T. Brunk[2], Chiara Urani[3], Pasquale Melchioretto[3], Gabriella Bonelli[1], Francesco M. Baccino[1] and Riccardo Autelli[*,1]

[1]Department of Clinical and Biological Sciences, University of Turin, Turin, 10125 Italy;
[2]Division of Pharmacology, Faculty of Health Sciences, Linköping University, Linköping, 58185 Sweden;
[3]Department of Earth and Environmental Sciences, University of Milan Bicocca, Milan, 20126 Italy

Abbreviated title:
Autophagy of metallothioneins prevents TNF toxicity

[*]**Corresponding author:**
Riccardo Autelli Ph.D.
Department of Clinical and Biological Sciences
University of Turin
Corso Raffaello 30
10125 Turin, Italy
Phone: +39 011 6707761
FAX: +39 011 2367761
e-mail: riccardo.autelli@unito.it

Keywords

Autophagy; cell death; hepatoma cells; oxidative stress; iron; lysosomes; TNF.

Abbreviations: AO, acridine orange; ApoF, apoferritin; HBSS, Hank's balanced salt solution; CHX, cycloheximide; DCF-DA, dichlorofluorescein diacetate; Dfp, deferiprone; LMP, lysosomal membrane permeabilization; MT, metallothionein(s); PI, propidium iodide; TNF, tumor necrosis factor; tfLC3, tandem fluorescent microtubule-associated protein 1A/1B-light chain 3-green/red fluorescent proteins chimera; TNFR1 and 2, TNF receptor 1 and 2.

Abstract

Lysosomal membrane permeabilization (LMP) induced by oxidative stress has recently emerged as a prominent mechanism behind TNF cytotoxicity. This pathway relies on diffusion of hydrogen peroxide into lysosomes containing redox-active iron, accumulated by breakdown of iron-containing proteins and subcellular organelles. Upon oxidative lysosomal damage, LMP allows relocation to the cytoplasm of low mass iron and acidic hydrolases that contribute to DNA and mitochondrial damage, resulting in death by apoptosis or necrosis. Here we investigate the role of lysosomes and free iron in death of HTC cells, a rat hepatoma line, exposed to TNF following metallothionein (MT) upregulation. Iron-binding MT does not normally occur in HTC cells in significant amounts.

Intracellular iron chelation attenuates TNF/cycloheximide (CHX)-induced LMP and cell death, demonstrating the critical role of this transition metal in mediating cytokine lethality. MT upregulation, combined with starvation-activated MT autophagy almost completely suppresses TNF/CHX toxicity, while impairment of both autophagy and MT upregulation by silencing of ATG7 and MT1A and/or 2A, respectively, abrogates protection. Interestingly, MT upregulation by itself has little effect, while stimulated autophagy alone depresses cytokine toxicity to some degree. These results provide evidence that intralysosomal iron-catalyzed redox reactions play a key role in TNF/CHX-induced LMP and toxicity. The finding that chelation of intralysosomal iron achieved by autophagic delivery of MT, and to some degree probably of other iron-binding proteins as well, into the lysosomal compartment is highly protective provides a putative mechanism to explain autophagy-related suppression of death by TNF/CHX.

Word count: 241

Introduction

TNF-mediated activation of TNF receptors 1 and 2 (TNFR1; TNFR2) is a powerful inducer of apoptosis/necrosis *in vivo* and *in vitro*. Initially, the death-inducing capability of this cytokine was believed to affect malignant cells only. Later, however, TNF was also found to affect hepatocytes and several other normal cells, and to be active in a number of disorders characterized by cell death and heavy inflammation.[1, 2] The mechanisms by which TNF exerts its effects have been intensely investigated and, at least to some degree, clarified. The TNF-binding capability of TNFR2 was demonstrated more than fifteen years ago,[3] but the full biological role of this receptor remains elusive. It is believed to propagate pro-survival[4] as well as cytotoxic[5] signals, the latter in synergism with TNFR1, which clearly transduces both forms of signals. TNF toxicity was initially accounted for by induction of caspase-dependent apoptotic death,[6] but later alternative non-necrotic, caspase-independent apoptotic-like death mechanisms were reported with increasing frequency.[7, 8]

As ligation of TNF to its two receptors induces both pro- and anti-survival signals, cytotoxicity often becomes less evident, probably as a consequence of NF-kB-dependent upregulation of a number of protective proteins that interfere with cell death programs. TNF toxicity, therefore, may not disclose itself unless the synthesis of such survival factors is restrained.[9-12] It is known that cycloheximide (CHX) and actinomycin D sensitize various cells to TNF, including hepatocytes and hepatoma cells.[13] While most of the known survival factors obstruct caspase-dependent death, others presumably act by different mechanisms. Depending on which death mechanisms TNF triggers, death-suppressing factors may vary substantially.

It is presently well known that the lysosomal compartment is involved in TNF cytotoxicity[14, 15] and that lysosomal membrane permeabilization (LMP) may induce apoptosis/necrosis.[16] Thus, at least some factors protecting against TNF might be proteins that safeguard the stability of lysosomes. Due to their common content of redox-active iron, a result of autophagic degradation of ferruginous materials (such as ferritin and mitochondria), lysosomes are often exposed to iron-

dependent oxidative reactions, including Fenton-type chemistry.[17, 18] These are mainly prevented by limiting the availability of lysosomal free Fe(II). This may occur following autophagy of iron-binding proteins, such as apoferritin, metallothioneins and HSP70, which all suppress LMP caused by oxidative stress.[19-21] The lysosomal presence of low mass labile iron represents a hazard in aerobic cells which produce superoxide and hydrogen peroxide that may diffuse into the lysosomal compartment and initiate Fenton-type reactions.

We previously reported that HTC cells, a rat hepatoma line, are killed by TNF in combination with sub-lethal concentrations of cycloheximide, but are protected by chelation of intracellular redox-reactive iron.[22] More recently, we showed that TNF/CHX-induced death is mediated by LMP.[23, 24] These findings indicate that, indeed, intralysosomal iron, oxidative stress and LMP all contribute to TNF toxicity. In the present study, we further investigate the role of lysosomal iron and LMP following exposure of rat hepatoma cells to TNF/CHX. We show that upregulation of iron-binding metallothionein(s) (MT) in combination with starvation-activated autophagy suppresses TNF toxicity.

Results

Role of iron in LMP and apoptosis-like death of HTC cells by TNF/CHX. In order to find out whether lysosomal iron is important in TNF/CHX-induced death, we exposed HTC cells for 2 h to a precipitate of hydrated iron phosphate, obtained by adding $FeCl_3$ to the medium. The formed insoluble Fe-phosphate is endocytosed and distributes within the lysosomal compartment.[25] While not toxic by itself even at the highest concentration used (200 μM), added iron dose-dependently enhanced TNF/CHX-induced LMP (**Fig. 1A**).

We previously reported that iron chelation by desferrioxamine partly protects HTC cells from TNF/CHX-induced death.[22] In the present work, before TNF/CHX exposure, cells were incubated for 18 h with the low molecular weight, water-soluble, iron chelator deferiprone, or for 4 h with apoferritin. Flow cytometry was used to evaluate both the fraction of annexin V-positive/propidium iodide-negative apoptotic cells and, following exposure to acridine orange (AO), the proportion of 'pale' cells, namely of those exhibiting lower red fluorescence than controls (**Fig. 1B**). This change reflects a reduced number of intact lysosomes, which all display intense red fluorescence, and is a reliable marker of LMP.[26] While apoferritin only partly protected from TNF/CHX-induced death and LMP, deferiprone almost completely prevented both lysosomal alterations and phosphatidylserine externalization in agreement with our earlier reports.[22] In our system, moderate LMP was an early and asynchronous event distinct from necrosis and associated with moderate cell shrinkage. Cells showing low to moderate LMP retained plasma membrane integrity and did not take up the GelGreen dye (**Fig. 1C**, arrowheads), indicating that necrosis is not yet occurring at this stage. By contrast, highly condensed cells, showing diffuse LysoTracker Red staining (necrotic cells), also displayed intense green fluorescence (**Fig. 1C**, arrow). These data are in good agreement with our previous results and those of other groups and support the view that LMP is a major effector mechanisms of TNF/CHX-induced death, and not a mere consequence of death itself.

Involvement of lysosomes in TNF/CHX-induced alterations of intracellular redox homeostasis. As the presented results strongly suggest that iron actively mediates TNF/CHX-induced cell death, the redox status of cytokine-treated HTC cells was evaluated by means of dichlorofluorescein diacetate (DCF-DA). This ester freely permeates the plasma membrane; in the cytoplasm it is split by non-specific esterases to yield a non-membrane permeable alcohol (DCF), which turns highly green-fluorescent if oxidized by hydroxyl radicals or peroxidase reactions.[27] In controls, only a few cells (**Fig. 2A**, upper panels) appeared rounded up and showed intense fluorescence, probably representing dying cells in which Fenton-like reactions occur owing to relocation of redox-active iron from bursting lysosomes to the cytoplasm in combination with production of hydrogen peroxide from damaged mitochondria. TNF/CHX markedly affected the morphology of cells, some of which exhibited either intense or low green fluorescence (**Fig. 2A**, lower panels, arrowheads and arrows, respectively), confirming that the cellular redox status was altered by TNF/CHX. Interestingly, many of these cells displayed a characteristic punctate fluorescence, yet not all cells undergoing morphological alterations stained positive for DCF, presumably indicating that redox perturbations occurred asynchronously in the population, as already observed for LMP (see **Fig. 1C**). Cells displaying such a punctate pattern of DCF positivity were moderately shrunk, but clearly not yet necrotic as they still effectively excluded PI (**Fig. 2B**). The latter dye, however, freely permeated the highly condensed cells, which also were totally devoid of granular DCF fluorescence. TNF/CHX-induced granular DCF fluorescence markedly differed from that generated by H_2O_2, used as a positive control to induce oxidative stress, in which a strong and diffuse DCF fluorescence was observed, with no evidence of any punctate pattern (not shown). This difference suggests that, in TNF/CHX-treated cells, the outbreak of oxidative stress was initiated in specific areas of the cytoplasm. Coupled with the requirement of a functional acidic compartment for TNF/CHX toxicity,[22] this finding suggested that the fluorescent dots highlighted by DCF might be lysosomes. To clarify this point, cells treated with TNF/CHX were subsequently

stained with both DCF-DA and LysoTracker Red, a fluorescent probe for the lysosomal compartment. Only red fluorescence identifying intact lysosomes was detectable in control cells, with no positivity for DCF (**Fig. 2C**, upper panels). By contrast, in TNF/CHX-treated cells many LysoTracker-positive dots (lysosomes) were also positive for DCF, thus appearing yellowish in overlays (**Fig. 2C**, lower panels). This observation confirms that the lysosomal compartment was engaged in an intense redox activity consequent to treatment with TNF/CHX. Of interest, a few red-stained lysosomes were invisible when viewed under blue light to detect the green fluorescence of oxidized DCF (**Fig. 2C**, lower panels, white arrows), indicating that no oxidative reactions took place in those organelles. This suggests that TNF/CHX do not uniformly affect all lysosomes and that the co-staining may be a consequence of early and partial permeabilization of the membrane of particularly iron-rich lysosomes allowing the hydrophilic alcohol DCF to enter before lysosomal stability is completely lost.

Effects of starvation-enhanced autophagy on TNF/CHX toxicity. To analyze the role of autophagy on TNF toxicity, cells were starved by incubation in Hank's balanced salt solution (HBSS) for 2 h before being exposed to TNF/CHX. Starvation markedly stimulated autophagic flux, as demonstrated by increased number of autophagosomes and autolysosomes/cell (yellow and red puncta, respectively; **Fig. 3A**), and the degradation of SQSTM1/p62 (**Fig. 3B**), which was totally abrogated by a mixture of the lysosomal cathepsins B, H and L inhibitors E-64-d/leupeptin. Starvation-induced autophagy reduced TNF/CHX toxicity by about 40% (**Fig. 3C**), suggesting that some autophagocytosed cytoplasmic factors interfere with death signals triggered by TNF/CHX. Should this be the case, preventing intralysosomal degradation of autophagocytosed material would be expected to enhance starvation-associated protection. To test this possibility, starvation was performed in the presence of NH_4Cl in order to impair lysosomal degradation without affecting the early stages of the autophagic process.[28] As expected, NH_4Cl further increased the protection conferred by starvation (**Fig. 3C**) and, though reducing the staining of cells with intact lysosomes,

markedly diminished the frequency of pale cells independently of concomitant starvation, thus confirming that inhibiting lysosomal degradation significantly affects TNF/CHX toxicity (**Fig. 3D**). Similar results were obtained when acidic proteolysis was blocked by bafilomycin A1, a specific V-ATPase inhibitor that prevents lysosomal acidification (not shown). To confirm that the effect of NH_4Cl actually relies on impairment of lysosomal degradative activity, and not merely on their alkalinization, an E-64-d/leupeptin mixture was added simultaneously with starvation to selectively block acidic proteolysis. In keeping with NH_4Cl, the cathepsin inhibitors potentiated starvation-induced protection from TNF/CHX (**Fig. 3C**), thus supporting the view that blocking lysosomal degradation of autophagocytosed materials increases protection from death achieved by starvation-induced autophagy.

This finding strongly suggests that enforced autophagy and impaired intralysosomal degradation of autophagocytosed materials interfere with the propagation of TNF/CHX-related death signals.

Effect of metallothionein (MT) autophagy on TNF/CHX toxicity. The above findings suggest that starvation promotes the sequestration of iron-chelating proteins from cytoplasm into the lysosomal system. Since MT upregulation has been reported to protect against LMP induced by various kinds of oxidative stress,[29] we focused on this group of proteins, which bind a variety of metals, including iron [for a review see[30]] and, particularly, on the inducible 1A and 2A isoforms. The latter, in particular, are scarce in HTC cells and, therefore, upregulation of such proteins represents a suitable model to verify whether autophagy of iron-binding proteins may protect lysosomes and cells against oxidative stress. To test this hypothesis, we upregulated MTs by adding 50 μM $ZnCl_2$ to the growth medium for 24 h before ensuing starvation (or not) for 2 h and final treatment with TNF/CHX for 6 h. Exposure to $ZnCl_2$ increased the amount of both MT mRNAs (**Fig. 4A**), the 1A form markedly more than 2A (5 and 2 folds, respectively). The response of MT1A mRNA and protein to $ZnCl_2$ in the range of 50 - 100 μM was dose-dependent (**Fig. 4B**). Of

interest, 50 μM $ZnCl_2$ affected neither the starvation-induced degradation of SQSTM1, nor its prevention by E-64-d/leupeptin. This indicates that neither autophagy nor lysosomal proteolysis was affected by $ZnCl_2$ treatment (**Fig. 4C**). We next investigated whether, following starvation, upregulated MT is actually autophagocytosed and transferred to lysosomes. To this purpose, a plasmid encoding human MT2A-GFP was transfected together with a reliable autophagosomal marker.[31] Cells were then left untreated (**Fig. 4D**) or starved for 2 h as described (**Fig. 4E**), permeabilized with digitonin[32] and imaged using a confocal microscope. In controls, red fluorescence resulting from hMT2A-mCherry was dispersed all over the optical section, indicating no specific colocalization of this protein with the autophagosomes (green-fluorescent, due to LC3-GFP). Starvation brought about the formation of several cytoplasmic clusters of yellow dots (**Fig. 4E**, arrowheads), indicating colocalization (43.13 ± 4.3 % colocalization, as compared to 1.8 ± 2.5 % for controls) of hMT2A and the autophagosomal marker in identical regions of the analyzed optical sections. Such a colocalization, therefore, demonstrates that hMT2A is actually autophagocytosed by HTC cells following starvation.

To further investigate whether autophagic flux stimulated by starvation may allow the transfer of MT from autophagosomes to lysosomes, cells were transfected with both MT2A-GFP and the lysosomal marker LAMP1-mRFP, either left untreated (**Fig. 4F**) or starved for 2 h as described (**Fig. 4G**). In control cells, the green fluorescence of MT2A-GFP was evenly widespread all over the focal plan and unrelated to the LAMP1-mRFP signal, which, as expected, clustered in discrete red dots representing lysosomes. Starvation in the presence of lysosomal inhibitors gave rise to several red-fluorescent organelles (**Fig. 4G**, arrows), with an intensely green-fluorescent content, indicating the presence of MT2A. As MT was found to be autophagocytosed following starvation (**Fig. 4E**), its association to large vesicular LAMP1-positive organelles (28.7 ± 10. 1 % colocalization, compared to 0 % for non-starved cells) suggests that enlarged lysosomes, deriving from the blockade of acidic proteolysis by the used lysosomal inhibitors, also carry a significant

amount of MT2A-GFP chimera. This finding thus confirms that starvation-induced autophagic sequestration of MT actually takes place and precedes its subsequent delivery to lysosomes.

Eventually, the biological effect of MT upregulation and autophagy on TNF/CHX toxicity was investigated. Even minor MT upregulation, such as that achieved by the lowest $ZnCl_2$ concentration used, slightly attenuated TNF/CHX toxicity and LMP (**Fig. 4H** and **I**, respectively). Protection associated with MT upregulation alone was somewhat lower than that achieved by starvation alone (**Fig. 4H**). However, when starvation-enhanced autophagy followed MT induction, it became nearly complete, indicating that TNF toxicity is almost fully abrogated by starvation-induced autophagy of previously upregulated metallothioneins.

The relevance of autophagy in suppressing TNF toxicity was further investigated by transiently silencing ATG7, a protein essential in triggering this process.[16] siRNA effectively decreased the amount of ATG7 mRNA, but not that encoding for MT1A and 2A. Also MT upregulation by 50 μM $ZnCl_2$, which increased MT1A and 2A mRNAs by about 5.5 and 1.5 folds, respectively, was totally unaffected by silencing (**Fig. 5A**). ATG7 silencing, however, markedly impaired starvation-induced autophagic flux as evidenced by the markedly depressed number of autophagosomes and autolysosomes/cell formed following 2 h of starvation (**Fig. 5B**). As expected, impaired autophagy consequent to ATG7 silencing abrogated the protection from TNF toxicity conferred by starvation, either alone or following MT upregulation (**Fig. 5C**). We also investigated whether autophagy plays any role in Fe-induced sensitization to TNF (see **Fig. 1A**). To this aim, mock- and ATG7-silenced cells were treated with TNF/CHX in the presence of increasing amounts of unsoluble $FeCl_3$. Extensively pale cells were then quantified by flow cytometry. ATG7 silencing did not substantially modify the capability of Fe to sensitize HTC cells to TNF/CHX-induced LMP (**Fig. 5D**). This result thus indicates that inhibition of autophagy does not interfere with sensitization to TNF/CHX due to endocytosis of the Fe-phosphate complex.

Eventually, the specific role of MTs in $ZnCl_2$-related protection of HTC against TNF/CHX was investigated by interfering with upregulation of either MT1A or 2A, or of both simultaneously,

by siRNA application before starvation and exposure to TNF/CHX. While a scrambled siRNA did not affect MT induction by $ZnCl_2$, MT1A- and MT2A-specific siRNAs effectively prevented MT upregulation, in particular when MT1A was affected (**Fig. 6A**). When silenced cells were subsequently exposed to TNF/CHX with or without starvation, siControl did not affect the overall response to the cytokine (**Fig. 6B**, black bars) with respect to non-silenced cells (as shown in **Fig. 4H**). By contrast, siRNAs targeting MT1A or MT2A, both combined (**Fig. 6B**, white bars) and separately (**Fig. 6C** and **D**, respectively) totally abrogated $ZnCl_2$-induced protection. Remarkably MT1A silencing increased susceptibility of HTC cells to TNF/CHX more markedly than MT2A silencing, suggesting a minor role for MT2A in protecting these cells against cytokine toxicity. Of interest, MT silencing, while effectively eradicating protection by $ZnCl_2$, did not affect that conferred by autophagy, probably due to persistent sequestration and lysosomal delivery of normally available cytoplasmic iron-binding proteins other than MT(s). These results, combined with those in which autophagy was restrained by ATG7 silencing, thus definitely support our hypothesis that lysosomal delivery of upregulated MT is the key mechanism by which autophagy protects HTC cells against TNF/CHX-induced death.

Discussion

Cell death is frequently, though not invariably, observed in eukaryotic cells exposed to TNF. Interestingly, the toxic effect often only occurs, or is at least much more pronounced when the cytokine is combined with inhibition of macromolecular synthesis.[33] Depending on cell type, TNF triggers either caspase-dependent or -independent death pathways [reviewed in[6, 34]]. Although caspase activation, as part of extrinsic or intrinsic apoptotic pathways, was earlier considered primarily responsible for TNF-induced death(s), accumulating evidences now suggest that in a number of cases TNF toxicity is independent from, yet possibly occurring together with, caspase activation.[13, 35, 36] Among caspase-independent deaths, mechanisms such as induction of oxidative stress and release of acidic proteases from lysosomes have been reported to play a significant role in TNF toxicity *in vivo* and *in vitro*.[2, 37-39] So far, the exact mechanisms by which TNF triggers oxidative stress and affects cells and organelles remain elusive.

We previously reported that TNF/CHX trigger apoptotic-like death in rat hepatoma cells that are significantly protected by drugs that raise lysosomal pH, by the iron chelator desferrioxamine and lipophilic antioxidants as well as by NADPH oxidase inhibitors.[22] Collectively, these findings suggest that intralysosomal iron and NADPH oxidase are major mediators of TNF toxicity, pointing to a prominent role of redox-centered reactions in TNF/CHX-induced death of hepatoma cells.

In the present study, we further demonstrate that TNF/CHX-induced LMP and ensuing cell death are slightly but significantly increased by incubating HTC cells in the presence of an iron-phosphate complex that is endocytosed and split in the acidic lysosomes, thereby increasing their content of low-mass, redox-active iron. By contrast, they are markedly attenuated by iron chelators such as deferiprone or apoferritin, both more effective than desferrioxamine that does not readily cross the plasma membrane but is taken up by endocytosis.[40] Iron availability thus appears critical in influencing HTC death, strongly supporting the notion that it plays a central role in TNF/CHX toxicity. Low-mass iron is well known to be physiologically available in lysosomes, mainly

deriving from the breakdown of autophagocytosed ferruginous materials,[25, 41] such as ferritin and mitochondria that carry the major share of intracellular iron.[42] Upon degradation of the protein backbone, bound iron is freed in the lysosomal lumen and kept in ferrous (Fe^{2+}) form by the low pH and the reducing environment of lysosomes.[17, 43] Its redox-reactive configuration makes intralysosomal iron very prone to participate in Fenton-like reactions in the presence of H_2O_2. In this context, iron chelation acts as a chain-breaking event that prevents initiation of harmful redox reactions. Many studies have convincingly demonstrated that iron chelation affords protection in a number of oxidative stress-based models of cell death.[44] This scenario seems plausible in this model as well, and is fully supported by our previous demonstration that diphenylene iodonium, a putative inhibitor of NADPH oxidase, disrupts TNF/CHX toxicity.[22] TNF is known to activate NADPH oxidase in different cell types.[45, 46] In professional phagocytes its presence in plasma- and lysosomal membranes[47] is reported to account for intralysosomal Fenton-type reactions.[44] Superoxide produced by NADPH oxidase, inside or outside the lysosomal compartment, is rapidly dismutated to hydrogen peroxide that in turn would react with lysosomal free Fe^{2+}. If extensive, the oxidative process might propagate to the lysosomal membrane, where lipid peroxidation results in LMP and release of lysosomal contents, namely acidic hydrolases and low mass redox-active iron, into the cytoplasm.[48] Simultaneous staining by DCF and LysoTracker Red indicates that many, but not all lysosomes undergo a burst of oxidative reactions, which likely account for LMP. Importantly, this finding shows that lysosomes are differently sensitive to oxidation, probably because of different contents or redox-active iron.[19, 49] Lysosomal retention of LysoTracker Red for some time after initiation of oxidative stress witnesses that pronounced LMP is not an early event. Initially, only partial LMP seems to occur, allowing hydrophilic DCF to enter some lysosomes, but also LysoTracker Red to remain intralysosomally, while the plasma membrane is still intact. Further progress of LMP allows the release of lysosomal contents to the cytoplasm, contributing to the complete loss of selective plasma membrane permeability.

The results suggest that, at least in HTC cells, intralysosomal oxidative activity is an early event during cellular response to TNF/CHX. The retention in many lysosomes of LysoTracker Red early in the apoptotic cascade indicates that lysosomal membranes are not yet fully permeabilized. Of interest, our data also show that, simultaneously, some lysosomes do not allow DCF to enter. The most likely explanation for this lysosomal heterogeneity, which has been pointed out before,[49] is that, within a given population, lysosomes may largely differ with respect to their content of iron. Based on the above considerations, it was highly expected that chelation of endo-lysosomal, redox-active iron would provide good protection against TNF/CHX.

In agreement with a number of reports showing that autophagy protects from oxidative damage,[50-52] starvation-enhanced autophagy significantly attenuated HTC cell death by TNF/CHX, while ATG7 silencing prevented this effect. These findings strongly suggest that an altered iron/iron chelator balance within lysosomes, for example due to increased autophagy of available Fe-binding proteins, probably mainly ferritin, might account for this effect. This hypothesis was strengthened by the observation that NH_4Cl and selective cathepsin inhibitors both markedly potentiated protection from death by delaying lysosomal breakdown of autophagocytosed iron-chelating proteins (by lysosomal alkalinization and cathepsin inhibition) and allowing time for expelling most low-mass iron from the lysosomal compartment. To further prove our hypothesis we upregulated cytoplasmic MTs, normally expressed to very low levels in HTC, by exposing them to zinc prior to starvation. MTs are a class of low-abundance cytoplasmic SH-rich proteins binding a variety of metals, iron included,[30] whose upregulation has been shown to be highly protective against a number of harmful conditions, in particular those in which oxidative stress is involved.[29, 53-57] These proteins are often overexpressed in various cancers, making them more resistant to irradiation and drugs that induce oxidative stress.[58] In the present work, MT1A and 2A were found poorly expressed in HTC cells under basal conditions, but were easily upregulated by $ZnCl_2$. We also provide evidence that transiently overexpressed MT2A-GFP is sequestered in autophagosomes during starvation-induced autophagy and that some of it eventually relocalizes to lysosomes. Thus,

autophagic flux actually redirects cytoplasmic MTs to the lysosomal compartment, where they will chelate intralysosomal redox-active iron, suppress LMP and protect cells from TNF/CHX-induced death. In agreement with these results, selective targeting of this protective mechanism, namely MT upregulation and their autophagy-mediated relocation to the acidic compartment, significantly restrain resistance of HTC to TNF/CHX toxicity. As expected, MT1A and 2A silencing abrogated protection afforded by Zn, while that due to starvation alone was mainly unaffected. In keeping with the above results, we further provide evidence that ATG7 silencing counteracted the almost full protection brought about by starvation-enhanced autophagy of MT. Interestingly, in rat liver, degradation of this class of iron-binding proteins is accounted for mostly by the lysosomal cathepsins B and L.[59, 60] Consequently, inhibition of lysosomal proteolysis achieved by either NH_4Cl or the cathepsins B and L inhibitors E-64-d/leupeptin potentiated protection brought about by starvation, presumably by slowing down lysosomal degradation of autophagocytosed MTs. Of interest, the lowest zinc concentration used only weakly upregulated MTs and by itself only slightly protected from death, yet in combination with starvation-induced autophagy gave rise to a nearly total protection against TNF/CHX. This observation demonstrates that coupling upregulation of iron-binding proteins with autophagy is needed to disrupt the redox events that lead to LMP and death.

Collectively, the present results demonstrate that MT upregulation in combination with its enforced autophagic relocation to the lysosomal compartment is very effective in protecting HTC cells from the toxic effects of TNF/CHX. Therefore, the results also demonstrate that lysosomal iron-centered redox reactions largely account for TNF/CHX-induced LMP and toxicity and that oxidative stress is a major mechanism of TNF toxicity in HTC hepatoma cells.

Materials and Methods

Cell cultures and treatments. The HTC, a rat hepatoma cell line, were grown in a 1:1 mixture of DMEM/Ham's F12 medium (Sigma-Aldrich, D6421) supplemented with 10% FBS (Gibco, 10270106), 2 mM glutamine (Sigma-Aldrich, G3126), 100 U/ml penicillin and 100 µg/ml streptomycin (Sigma-Aldrich, P4333) in 95% humidified air with 5% CO_2. For experiments, cells were seeded at 10^4 cells/cm^2 and 18 h later exposed to 20 ng/ml TNF (R&D Systems, Minneapolis, 210-TA) plus 10 µg/ml CHX (Sigma-Aldrich, C7698) for 6 h. For MT upregulation, cells were incubated for 24 h with various concentrations of $ZnCl_2$ (Sigma-Aldrich, 429430). Autophagy was stimulated by starvation for 2 h in HBSS supplemented with 0.31% glucose at 37 °C, after which they were returned to standard growth conditions and further treated as above. Deferiprone and apoferritin (Sigma-Aldrich, 379409 and A3660, respectively) were dissolved in growth medium and added at the indicated concentrations 18 and 4 h before TNF/CHX treatment, respectively.

Quantification of MT1A, -2A and ATG7 mRNAs by real time RT-PCR. To evaluate the levels of the above transcripts, total RNA was extracted with the TriPure Isolation Reagent (Roche Diagnostics, 11667157001); 1 µg total RNA was reverse-transcribed in a 20 µl reaction using the Reverse Transcription System (Promega, A3500). Real time PCR was performed on 50 ng cDNA using the iQ SYBR Green Supermix (BioRad Laboratories, 170-8880) and an iCycler. Primers used (forward and reverse primer) were: MT1A: 5'-CCAACTGCTCCTGCTCCAC-3' and 5'-GAGGCACCTTTGCAGACACA-3'; MT2A: 5'-ATGGACCCCAACTGCTCCT-3' and 5'-GCACTTGTCCGAAGCCTCTT-3'; ATG7: 5'-ACCCTGCACAACACCAACAC-3' and 5'-GAGCATGGGGTTTTCGAGAG-3'. Normalization was performed with respect to the total amount of rat GAPDH mRNA for each sample as detected with the following primers: 5'-CCACTCAGAAGACTGTGGATGG-3' and 5'-GGATACATTGGGGGTAGGAACA-3'. The relative change of mRNAs under the various conditions was calculated using the $2^{-\Delta\Delta C_T}$ method.

Determination of autophagic flux. The effect of starvation on autophagic flux was assayed by transfecting the cells with the ptfLC3 plasmid[61] (Addgene plasmid 21074). Cells were plated at 8 x 10^3 cells/cm^2 onto a μ-Slide VI (Ibidi GmbH, 80606) and transfected 18 h later with 2 μg of the plasmid with Lipofectamine 2000 (Invitrogen, 11668-019). About 30 μl of DNA complex was added to each channel of the μ-Slide in antibiotic-free medium for 24 h to both control and ATG7-silenced cells. The next morning, cells were washed twice with PBS and returned to standard culture conditions for another 24 h before being starved as described above. Following starvation, cells were rinsed once with PBS, fixed for 20 min with 4% formaldehyde and rinsed twice with PBS before confocal examination. Samples were analyzed with a Leica TCS SP5-AOBS 5-channel confocal system (Leica Microsystems) equipped with a 405-nm diode, an argon ion, a 561-nm DPSS, and a 633-nm HeNe laser. Images were acquired using a HCX PL APO 63x/1.4 NA oil immersion objective at a pixel resolution of 240 x 240 or 80 x 80 nm and further processed with Photoshop 7.0. In order to make counting of autophagosomes and autolysosomes (yellow and red fluorescent dots, respectively) reliable and basically independent of the operator,[62] the Green and Red Puncta Colocalization ImageJ Plugin (created by Daniel J. Shiwarski, University of Pittsburgh; enhanced and modified by Ruben K. Dagda, University of Nevada School of Medicine and co-approved as an image tool for autophagic flux by Charleen T. Chu, University of Pittsburgh), was used without any setting change or adjustment on a number (indicated in each relevant histogram) of single-cell images extracted from different microscopic fields (3 to 6 for each experimental condition).[63]

Autophagy and lysosomal delivery of MT. For detection of MT autophagy, a construct (pcDNA3-hMT2A-mCherry) encoding a human MT2A-mCherry was generated by ligase-independent cloning of the MT2A cDNA (PCR-amplified from pcDNA3-GFP-hMT2A; Addgene plasmid 11613) into the pcDNA3-mCherry LIC cloning vector (6B) (Addgene plasmid 30125). pcDNA3-hMT2A-mCherry was cotransfected with the autophagosomal marker pEGFP-C1-LC3. For analysis of

lysosomal delivery of MT, the pcDNA3-GFP-hMT2A was cotransfected with the lysosomal marker pLJM1-LAMP1-mRFP-FLAG (Addgene plasmid 34611).

For transfections, cells were seeded at the density of 3 x 10^3/cm^2 in individual wells of µ-Slides 8 wells (Ibidi GmbH, 80826, ibiTreat) and transfected 24 h later with 0.4 µg of the above constructs with Lipofectamine 2000 in antibiotics-free medium (DNA:Lipofectamine 2000 ratio of 1:0.75). The next morning cells were returned to complete growth medium for an additional period of 24 h. Cells were then pretreated with 100 µM E-64-d (Santa Cruz Biotechnology, sc-201280) plus 10 µM leupeptin (Enzo Life Science, ALX-260-009) for 60 min, after which they were starved for 2 h in HBSS/glucose in the presence of the above inhibitors plus 1 µM bafilomycin A1 (Adipogen, BVT-0252), added to the starvation medium without any pretreatment. During starvation, cells were stained for 60 min with 0.5 µg/ml Hoechst 33258 (Sigma-Aldrich, 861405). Before fixation, cells were permeabilized for about 1 (controls) or 2-3 (starved cells) min with 100 µg/ml digitonin in PBS (Sigma-Aldrich, D5628) at room temperature. This method is a modification of the original saponin-based technique.[32] The setting of permeabilization conditions was performed by monitoring the increase of red fluorescence following incubation of cells for 2 min with increasing concentrations of digitonin in the presence of 20 µg/ml of propidium iodide (Sigma-Aldrich, P4170). A concentration of 100 µg/ml digitonin was chosen as it resulted in a positivity of more than 95% cells to PI as evaluated by FACS analysis (not shown). Shorter permeabilization of controls was required in order to show the expression of transfected hMT2A, using either the -mCherry or -GFP variant, as a longer permeabilization totally released the protein not segregated inside the autophagosomes or lysosomes by starvation. After permeabilization, cells were fixed with 4% formaldehyde for 20 min and stored for confocal analysis; recorded images were composed with Photoshop 7.0 as described above.

Colocalization analysis was performed with the JACoP[64] tool for ImageJ (using the 'object-based' method) on at least 5 single cells extracted from independent microscopic fields.

Detection of lysosomal oxidative activity. For detection of oxidative stress, cells were treated with TNF/CHX as above, or with 10 mM H_2O_2 (initial concentration; Sigma-Aldrich, H1009) for 30 min in PBS as a positive control, followed by another 5.5 h recovery in complete growth medium under standard culture conditions. Cells were then loaded with 10 μM dichlorofluorescein diacetate (DCF-DA; Sigma-Aldrich, D6883) for 30 min, in growth medium without phenol red. When simultaneous detection of the lysosomal compartment was required, 25 nM LysoTracker Red was added 10 min after start of staining with DCF-DA. Cells were then exposed to both tracers for another 10 min. Total DCF-DA loading time was thus shortened to 20 min to increase the ratio of puncta to cytoplasm staining. Residual dye was removed by a medium change. Following addition of fresh growth medium, cultures were promptly imaged using an inverted fluorescence microscope and representative pictures acquired and composed as described above.

Flow cytometric quantification of apoptosis. Frequency of apoptotic cells was estimated by counting the percentage of phosphatidylserine-positive/propidium iodide (PI)-negative cells using the Annexin V/PI kit (ImmunoStep, DY-634). Adherent cells were lifted with 0.25% trypsin and collected together with floating ones, centrifuged and resuspended in 190 μl of binding buffer (10 mM HEPES-NaOH pH 7.4, 140 mM NaCl, 2.5 mM $CaCl_2$) before addition of annexin V and PI. A total of 5,000 cells were analyzed in a FACScan equipped with a 488 nm argon laser using the CellQuest software (Becton-Dickinson).

Lysosomal membrane permeabilization assay. Lysosomal membrane permeabilization (LMP) was assayed with the acridine orange (AO) uptake technique.[26] Following treatments, cells were loaded for 15 min at 37 °C with 5 μg/ml AO (final concentration) in complete growth medium. Attached and floating cells were collected and resuspended in 200 μl of PBS. AO fluorescence from 10,000 cells/sample was measured by flow cytometry, as described above. Cells with lowest red

fluorescence ('pale' cells, indicating cells with a diminished number of intact lysosomes) were recorded.

Detection of plasma membrane permeabilization. Detection of plasma membrane permeabilization in cells showing LMP was accomplished with GelGreen (Biotium, 41005). Briefly, cells were treated or not with TNF/CHX and stained with LysoTracker Red as described. GelGreen was then added at a final dilution of 1:10,000 and incubated for additional 10 min at 37 °C in complete growth medium to allow a good staining of necrotic cells. When plasma membrane permeability was investigated in cells loaded with DCF-DA, 30 μg/ml of propidium iodide was added to the growth medium just before microscopic analysis. In both cases, the cultures were observed, and representative pictures captured and imaged as described above.

Downregulation of MT1A, 2A and ATG7 by RNA interference. MT1A and 2A silencing was obtained by transfecting HTC cells with 15 pmoles (50 nM final concentration) of a Mission predesigned siRNA (Sigma-Aldrich, SASI_Rn01_00065310 for MT1A and SASI_Rn01_00332519 for MT2A) with Metafectene Pro (Biontex, T040). As higher concentrations of MT-targeting siRNAs were highly toxic to these cells, for simultaneous silencing of both MT1A and 2A 10 and 5 pmoles of each siRNA were used per each well, respectively, thereby keeping the total siRNA concentration as low as 50 nM. Cells were incubated with the indicated amounts of each siRNA for 72 h; 50 μM $ZnCl_2$ was added following 48 h of transfection and left for another 24 h. Medium was then changed to either normal growth medium or to HBSS for starvation for 2 h, after which cells were exposed to TNF/CHX as described.

ATG7 silencing was achieved by targeting the rat isoform. HTC cells were transfected for 72 h in complete growth medium with 30 pmoles (100 nM final concentration) of a Mission predesigned siRNA (Sigma-Aldrich, SASI_Rn01_00050326) using MefactenePro. siRNA with random sequence were used as a control reaction at the same concentration and with the same

administration schedule. Then, after a change of medium, cells were treated with TNF/CHX as indicated. All siRNAs used for these experiments (MT1A, 2A and ATG7) were maintained in the medium during all treatments, namely MT induction with 50 μM $ZnCl_2$ for 24 h, starvation for 2 h in HBSS and TNF/CHX treatment for 6 h.

Western blot analysis of MT and SQSTM1/p62. MT detection was performed essentially as described.[65] Briefly, control and $ZnCl_2$-exposed cells were scraped from the growth flasks, washed with PBS and centrifuged at 100 RCF for 10 min at 4 °C. Pellets were resuspended with 10 mM TRIS-Cl, pH 7.0, 5 mM EDTA containing 1 mM PMSF and immediately frozen at -80 °C to obtain complete cell rupture. Defrosted samples were then centrifuged at 20,000 RCF for 45 min at 4 °C; 30 μg of each sample was fractionated on a 12% NuPAGE gel (Invitrogen, NP0341), transferred and fixed to nitrocellulose according to Mizzen *et al.*[66] An overnight incubation with a primary mouse monoclonal antibody against metallothionein-I and -II (1:1,000, Zymed Laboratories Inc., 18-0133) was followed by 4 h of incubation with an alkaline phosphatase-conjugated secondary antibody (1:1,000, Sigma-Aldrich, A4312) and a chromogenic substrate (BCIP/NBT, Sigma-Aldrich, 72091) for visualization of the bands.

For analysis of SQSTM1 degradation, aliquots of 20 μg of total lysates from controls and cells treated with 100 μM E-64-d plus 10 μM leupeptin were fractionated on a 12% acrylamide gel and transferred to nitrocellulose. Membranes were then probed with an anti-SQSTM1 antibody (Sigma-Aldrich, P0067) for 60 min at 4 °C. As a control for loading, membranes were subsequently probed with a mouse monoclonal anti-β-actin antibody (clone AC-15; 1:4,000, Sigma-Aldrich, A5441), and washed with 0.05% TBS-Tween. After incubation with an anti-IgG antibody (1:10,000, Bio-Rad Laboratories, 172-1011 or 170-6515) chemiluminescent detection was performed with the ImmunoCruz Western Blotting Luminol Reagent (Santa Cruz Biotechnology, sc-2048).

Statistical analysis. Data represent means ± SD from at least three independent experiments, each assayed in triplicate. Differences between groups were analyzed either by one-way ANOVA followed by Student-Newman-Keuls post-test or by the Student's t test using Instat (Ver. 3.01, GraphPad).

Disclosure of potential conflicts of interest

No potential conflicts of interest were disclosed.

Acknowledgments

This work was supported by grants from Ministero dell'Università e della Ricerca and Università degli Studi di Torino. We are grateful to Prof. Tamotsu Yoshimori, Graduate School of Medicine, Osaka, JPN, Prof. Steven Johnson, Oregon Health and Science University, Portland, OR, USA and Prof. David Sabatini, Department of Biology, Massachusetts Institute of Technology, Cambridge, USA, for having kindly provided us with the constructs encoding for the tfLC3, GFP-MT2A and for the mCherry-LIC (6B) backbone, respectively; to Prof. John W. Eaton, University of Louisville, KY, USA, for his critical reading of the manuscript and valuable suggestions and to Prof. Ana Maria Cuervo, Albert Einstein College of Medicine, NY, USA, for valuable suggestions on ATG protein silencing.

References

1. Bradley JR. TNF-mediated inflammatory disease. J Pathol 2008; 214:149-60.
2. Schwabe RF, Brenner DA. Mechanisms of liver injury. I. TNF-alpha-induced liver injury: role of IKK, JNK, and ROS pathways. Am J Physiol Gastrointest Liver Physiol 2006; 290:G583-G589.
3. Grell M, Douni E, Wajant H, Löhden M, Clauss M, Maxeiner B, Georgopoulos S, Lesslauer W, Kollias G, Pfizenmaier K, et al. The transmembrane form of tumor necrosis factor is the prime activating ligand of the 80 kDa tumor necrosis factor receptor. Cell 1995; 83:793-802.
4. Rodriguez M, Cabal-Hierro L, Carcedo MT, Iglesias JM, Artime N, Darnay BG, Lazo PS. NF-kB signal triggering and termination by tumor necrosis factor receptor 2. J Biol Chem 2011; 286:22814-24.
5. Tartaglia LA, Pennica D, Goeddel DV. Ligand passing: the 75-kDa tumor necrosis factor (TNF) receptor recruits TNF for signaling by the 55-kDa TNF receptor. J Biol Chem 1993; 268:18542-8.
6. Scaffidi C, Fulda S, Srinivasan A, Friesen C, Li F, Tomaselli KJ, Debatin KM, Krammer PH, Peter ME. Two CD95 (APO-1/Fas) signaling pathways. EMBO J 1998; 17:1675-87.
7. Leist M, Jäättelä M. Four deaths and a funeral: from caspases to alternative mechanisms. Nat Rev Mol Cell Biol 2001; 2:589-98.
8. Lockshin RA, Zakeri Z. Caspase-independent cell deaths. Curr Opin Cell Biol 2002; 14:727-33.
9. Alessenko AV, Boikov PY, Filippova GN, Khrenov AV, Loginov AS, Makarieva ED. Mechanisms of cycloheximide-induced apoptosis in liver cells. FEBS Lett 1997; 416:113-6.
10. Duriez PJ, Wong F, Dorovini-Zis K, Shahidi R, Karsan A. A1 functions at the mitochondria to delay endothelial apoptosis in response to tumor necrosis factor. J Biol Chem 2000; 275:18099-107.

11. Lüschen S, Ussat S, Scherer G, Kabelitz D, Adam-Klages S. Sensitization to death receptor cytotoxicity by inhibition of fas-associated death domain protein (FADD)/caspase signaling. Requirement of cell cycle progression. J Biol Chem 2000; 275:24670-8.
12. Warren S, Torti SV, Torti FM. The role of iron in the cytotoxicity of tumor necrosis factor. Lymphokine Cytokine Res 1993; 12:75-80.
13. Jones BE, Lo CR, Liu H, Srinivasan A, Streetz K, Valentino KL, Czaja MJ. Hepatocytes sensitized to tumor necrosis factor-alpha cytotoxicity undergo apoptosis through caspase-dependent and caspase-independent pathways. J Biol Chem 2000; 275:705-12.
14. Monney L, Olivier R, Otter I, Jansen B, Poirier GG, Borner C. Role of an acidic compartment in tumor-necrosis-factor-alpha-induced production of ceramide, activation of caspase-3 and apoptosis. Eur J Biochem 1998; 251:295-303.
15. Werneburg N, Guicciardi ME, Yin XM, Gores GJ. TNF-alpha-mediated lysosomal permeabilization is FAN and caspase 8/Bid dependent. Am J Physiol Gastrointest Liver Physiol 2004; 287:G436-G443.
16. Kroemer G, Jäättelä M. Lysosomes and autophagy in cell death control. Nat Rev Cancer 2005; 5:886-97.
17. Terman A, Kurz T. Lysosomal iron, iron chelation and cell death. Antioxid Redox Signal 2013; 18:888-98.
18. Terman A, Kurz T, Gustafsson B, Brunk UT. Lysosomal labilization. IUBMB Life 2006; 58:531-9.
19. Kurz T, Gustafsson B, Brunk UT. Cell sensitivity to oxidative stress is influenced by ferritin autophagy. Free Radic Biol Med 2011; 50:1647-58.
20. Kurz T, Brunk UT. Autophagy of HSP70 and chelation of lysosomal iron in a non-redox-active form. Autophagy 2009; 5:93-5.
21. Gyrd-Hansen M, Nylandsted J, Jäättelä M. Heat shock protein 70 promotes cancer cell viability by safeguarding lysosomal integrity. Cell Cycle 2004; 3:1484-5.

22. Autelli R, Crepaldi S, De Stefanis D, Parola M, Bonelli G, Baccino FM. Intracellular free iron and acidic pathways mediate TNF-induced death of rat hepatoma cells. Apoptosis 2005; 10:777-86.

23. Autelli R, Ullio C, Prigione E, Crepaldi S, Schiavone N, Brunk UT, Capaccioli S, Baccino FM, Bonelli G. Divergent pathways for TNF and C(2)-ceramide toxicity in HTC hepatoma cells. Biochim Biophys Acta 2009; 1793:1182-90.

24. Ullio C, Casas J, Brunk UT, Sala G, Fabriàs G, Ghidoni R, Bonelli G, Baccino FM, Autelli R. Sphingosine mediates TNFalpha-induced lysosomal membrane permeabilization and ensuing programmed cell death in hepatoma cells. J Lipid Res 2012; 53:1134-43.

25. Yu Z, Persson HL, Eaton JW, Brunk UT. Intralysosomal iron: a major determinant of oxidant-induced cell death. Free Radic Biol Med 2003; 34:1243-52.

26. Zhao M, Eaton JW, Brunk UT. Protection against oxidant-mediated lysosomal rupture: a new anti-apoptotic activity of Bcl-2? FEBS Lett 2000; 485:104-8.

27. Karlsson M, Kurz T, Brunk UT, Nilsson SE, Frennesson CI. What does the commonly used DCF test for oxidative stress really show? Biochem J 2010; 428:183-90.

28. Øverbye A, Sætre F, Hagen LK, Johansen HT, Seglen PO. Autophagic activity measured in whole rat hepatocytes as the accumulation of a novel BHMT fragment (p10), generated in amphisomes by the asparaginyl proteinase, legumain. Autophagy 2011; 7:1011-27.

29. Baird SK, Kurz T, Brunk UT. Metallothionein protects against oxidative stress-induced lysosomal destabilization. Biochem J 2006; 394:275-83.

30. Andrews GK. Regulation of metallothionein gene expression by oxidative stress and metal ions. Biochem Pharmacol 2000; 59:95-104.

31. Koyama-Honda I, Itakura E, Fujiwara TK, Mizushima N. Temporal analysis of recruitment of mammalian ATG proteins to the autophagosome formation site. Autophagy 2013; 9:1491-9.

32. Eng KE, Panas MD, Karlsson Hedestam GB, McInerney GM. A novel quantitative flow cytometry-based assay for autophagy. Autophagy 2010; 6:634-41.
33. Shishodia S, Aggarwal BB. Nuclear factor-kappaB activation: a question of life or death. J Biochem Mol Biol 2002; 35:28-40.
34. Vandenabeele P, Galluzzi L, Vanden BT, Kroemer G. Molecular mechanisms of necroptosis: an ordered cellular explosion. Nat Rev Mol Cell Biol 2010; 11:700-14.
35. Chipuk JE, Green DR. Do inducers of apoptosis trigger caspase-independent cell death? Nat Rev Mol Cell Biol 2005; 6:268-75.
36. Wilson CA, Browning JL. Death of HT29 adenocarcinoma cells induced by TNF family receptor activation is caspase-independent and displays features of both apoptosis and necrosis. Cell Death Differ 2002; 9:1321-33.
37. Dada LA, Sznajder JI. Mitochondrial Ca(2)+ and ROS take center stage to orchestrate TNF-alpha-mediated inflammatory responses. J Clin Invest 2011; 121:1683-5.
38. Kim JJ, Lee SB, Park JK, Yoo YD. TNF-alpha-induced ROS production triggering apoptosis is directly linked to Romo1 and Bcl-X(L). Cell Death Differ 2010; 17:1420-34.
39. Sakon S, Xue X, Takekawa M, Sasazuki T, Okazaki T, Kojima Y, Piao JH, Yagita H, Okumura K, Doi T, et al. NF-kappaB inhibits TNF-induced accumulation of ROS that mediate prolonged MAPK activation and necrotic cell death. EMBO J 2003; 22:3898-909.
40. Lloyd JB, Cable H, Rice-Evans C. Evidence that desferrioxamine cannot enter cells by passive diffusion. Biochem Pharmacol 1991; 41:1361-3.
41. Kurz T, Eaton JW, Brunk UT. The role of lysosomes in iron metabolism and recycling. Int J Biochem Cell Biol 2011; 43:1686-97.
42. Levi S, Rovida E. The role of iron in mitochondrial function. Biochim Biophys Acta 2009; 1790:629-36.
43. Brunk UT, Neuzil J, Eaton JW. Lysosomal involvement in apoptosis. Redox Rep 2001; 6:91-7.

44. Persson HL, Nilsson KJ, Brunk UT. Novel cellular defenses against iron and oxidation: ferritin and autophagocytosis preserve lysosomal stability in airway epithelium. Redox Rep 2001; 6:57-63.

45. Kim YS, Morgan MJ, Choksi S, Liu ZG. TNF-induced activation of the Nox1 NADPH oxidase and its role in the induction of necrotic cell death. Mol Cell 2007; 26:675-87.

46. Basuroy S, Bhattacharya S, Leffler CW, Parfenova H. Nox4 NADPH oxidase mediates oxidative stress and apoptosis caused by TNF-alpha in cerebral vascular endothelial cells. Am J Physiol Cell Physiol 2009; 296:C422-C432.

47. Chen CS. Phorbol ester induces elevated oxidative activity and alkalization in a subset of lysosomes. BMC Cell Biol 2002; 3:21-32.

48. Droga-Mazovec G, Bojic L, Petelin A, Ivanova S, Romih R, Repnik U, Salvesen GS, Stoka V, Turk V, Turk B. Cysteine cathepsins trigger caspase-dependent cell death through cleavage of bid and antiapoptotic Bcl-2 homologues. J Biol Chem 2008; 283:19140-50.

49. Nilsson E, Ghassemifar R, Brunk UT. Lysosomal heterogeneity between and within cells with respect to resistance against oxidative stress. Histochem J 1997; 29:857-65.

50. Czaja MJ. Two types of autophagy are better than one during hepatocyte oxidative stress. Autophagy 2011; 7:96-7.

51. Lv XC, Zhou HY. Resveratrol protects H9c2 embryonic rat heart derived cells from oxidative stress by inducing autophagy: role of p38 mitogen-activated protein kinase. Can J Physiol Pharmacol 2012; 90:655-62.

52. Marino ML, Fais S, Djavaheri-Mergny M, Villa A, Meschini S, Lozupone F, Venturi G, Della Mina P, Pattingre S, Rivoltini L, et al. Proton pump inhibition induces autophagy as a survival mechanism following oxidative stress in human melanoma cells. Cell Death Dis 2010; 1:e87. doi: 10.1038/cddis.2010.67.:e87.

53. Chiaverini N, De Ley M. Protective effect of metallothionein on oxidative stress-induced DNA damage. Free Radic Res 2010; 44:605-13.

54. Lu H, Hunt DM, Ganti R, Davis A, Dutt K, Alam J, Hunt RC. Metallothionein protects retinal pigment epithelial cells against apoptosis and oxidative stress. Exp Eye Res 2002; 74:83-92.

55. Weng CJ, Chen MJ, Yeh CT, Yen GC. Hepatoprotection of quercetin against oxidative stress by induction of metallothionein expression through activating MAPK and PI3K pathways and enhancing Nrf2 DNA-binding activity. N Biotechnol 2011; 28:767-77.

56. You HJ, Lee KJ, Jeong HG. Overexpression of human metallothionein-III prevents hydrogen peroxide-induced oxidative stress in human fibroblasts. FEBS Lett 2002; 521:175-9.

57. Lee SJ, Koh JY. Roles of zinc and metallothionein-3 in oxidative stress-induced lysosomal dysfunction, cell death, and autophagy in neurons and astrocytes. Mol Brain 2010; 3:30-8.

58. Pedersen MO, Larsen A, Stoltenberg M, Penkowa M. The role of metallothionein in oncogenesis and cancer prognosis. Prog Histochem Cytochem 2009; 44:29-64.

59. Choudhuri S, McKim JM, Jr., Klaassen CD. Role of hepatic lysosomes in the degradation of metallothionein. Toxicol Appl Pharmacol 1992; 115:64-71.

60. Klaassen CD, Choudhuri S, McKim JM, Jr., Lehman-McKeeman LD, Kershaw WC. In vitro and in vivo studies on the degradation of metallothionein. Environ Health Perspect 1994; 102 Suppl 3:141-6.

61. Kimura S, Noda T, Yoshimori T. Dissection of the autophagosome maturation process by a novel reporter protein, tandem fluorescent-tagged LC3. Autophagy 2007; 3:452-60.

62. Porter K, Nallathambi J, Lin Y, Liton PB. Lysosomal basification and decreased autophagic flux in oxidatively stressed trabecular meshwork cells: implications for glaucoma pathogenesis. Autophagy 2013; 9:581-94.

63. Chu CT, Plowey ED, Dagda RK, Hickey RW, Cherra SJ, III, Clark RS. Autophagy in neurite injury and neurodegeneration: in vitro and in vivo models. Methods Enzymol 2009; 453:217-49.

64. Bolte S, Cordelieres FP. A guided tour into subcellular colocalization analysis in light microscopy. J Microsc 2006; 224:213-32.

65. Urani C, Melchioretto P, Gribaldo L. Regulation of metallothioneins and ZnT-1 transporter expression in human hepatoma cells HepG2 exposed to zinc and cadmium. Toxicol In Vitro 2010; 24:370-4.

66. Mizzen CA, Cartel NJ, Yu WH, Fraser PE, McLachlan DR. Sensitive detection of metallothioneins-1, -2 and -3 in tissue homogenates by immunoblotting: a method for enhanced membrane transfer and retention. J Biochem Biophys Methods 1996; 32:77-83.

FIGURE LEGENDS

Figure 1. Iron affects TNF/CHX toxicity in HTC cells. (**A**) Cells were exposed for 2 h to a precipitate of hydrated iron-phosphate, which spontaneously forms when $FeCl_3$ is added to the medium, and subsequently treated with 20 ng/ml TNF plus 10 μg/ml CHX for another 6 h. Cells were then loaded for 15 min with acridine orange (AO) at a final concentration of 5 μg/ml in complete growth medium and analyzed by flow cytometry. 10,000 cells were run each time in a FACScan flow cytometer; data were collected and analyzed with the CellQuest software. 'Pale' cells represent the population with the lowest red fluorescence (as illustrated in Fig. 3D) when exposed to green light, due to a reduced number of normal lysosomes. (**B**) Cells were incubated with either 1 μM apoferritin (ApoF) for 4 h or 250 μM deferiprone (Dfp) for 18 h before being exposed to TNF/CHX for 6 h. At the end of treatment, the number of annexin V-positive/PI-negative cells (black bars) and of 'pale' cells (light gray bars) was measured on 5,000 and 10,000 cells per sample as described above. (**C**) Cells were treated with TNF/CHX as in (**A**), sequentially stained with LysoTracker Red and GelGreen as indicated in Materials and Methods and observed under a fluorescence microscope. The frame in the left panel (phase contrast) was electronically magnified and the red and green channels reproduced, either separately (middle two panels) or overlaid in the rightmost panel. Arrowheads indicate moderately shrunk cells undergoing initial LMP, but still retaining plasma membrane selective permeability, as is implied by their impermeability to GelGreen. The arrow points to a strongly condensed cell with fully permeabilized lysosomes, taking up the GelGreen dye, suggestive of a late phase of death ("late apoptotic" or "secondary necrotic" cell).

Data represent the means ± SD of at least three independent experiments. *, **, ***: $p < 0.05$, $p < 0.01$ and $p < 0.001$, respectively, *vs* TNF/CHX (ANOVA).

Figure 2. TNF/CHX exposure triggers redox reactions that involve the lysosomal compartment. (**A**) Cells were left untreated (top panels), or treated with TNF/CHX as in Fig. 1 (bottom panels).

Cultures were then exposed for 30 min to 10 μM dichlorofluorescein diacetate (DCF-DA) in medium without phenol red, rinsed with fresh growth medium and observed under an inverted fluorescence microscope. Cells with evident TNF/CHX-related morphological alterations displayed a lysosomal-type punctate intense fluorescence (arrowheads), while other cells, in which morphological changes were not yet so established displayed less intense green fluorescence (arrows), suggesting the process to still be in a very early phase. (**B**) Cells were treated with TNF/CHX and sequentially loaded with 10 μM DCF-DA as in (**A**) and, just before observation, stained with 30 μg/ml of PI. The green fluorescent cells (showing "granular" DCF-DA-positivity) do not take up PI, indicating that redox reactions occur in an early phase of the death process. (**C**) Cells were treated with TNF/CHX as in (**A**) and sequentially loaded with 10 μM DCF-DA and 25 nM LysoTracker Red DND-99 as described in Materials and Methods. Controls (upper panels) and cells treated with TNF/CHX (lower panels) were observed and photographed as in (**A**). Arrows indicate lysosomes that are not stained by DCF. The pictures shown in (**A-C**) are representative of three different experiments for each condition.

Figure 3. Induction of autophagy and inhibition of lysosomal proteolysis protect from TNF/CHX-induced death. (**A**) Cells were transfected with ptfLC3, starved in amino acid-free medium (HBSS containing glucose) for 2 h and examined with a confocal microscope (left panel) for quantification (histograms) of yellow and red fluorescent dots/cell representing autophagosomes and autolysosomes, respectively. Amino acid deprivation increases number and size of both autophagosomes and autolysosomes, suggestive of enhanced autophagic flux. The number of cells examined for autophagosomes/autolysosomes quantification is indicated in each bar. (**B**) The kinetics of SQSTM1 degradation was assayed by western blotting (left panel, representative of three independent experiments) under both control conditions and following starvation for 2 h in HBSS/glucose, in the absence or presence of 100 μM E-64-d and 10 μM leupeptin (E64d/Leu, for the full period of starvation), to inhibit lysosomal proteolysis. Normalization was performed against

the level of β-actin of each sample. The relative amount of SQSTM1 was expressed *vs* that of time 0 for each condition (histograms, right panel). (**C**) Cells starved as above for 2 h were exposed to TNF/CHX for 6 h in the absence or presence of 20 mM NH_4Cl, added during the last 60 min of starvation, or of 100 μM E-64-d and 10 μM leupeptin for the whole period of starvation. The percentage of apoptotic-like cells (phosphatidylserine-positive and PI-negative) was then quantified by flow cytometry (5,000 cells were analyzed for each sample). Only occasional necrotic (PI positive) cells were found. (**D**) Cells were exposed for 6 h to TNF/CHX following 2 h of starvation (upper panel) or 1 h of incubation with NH_4Cl (middle panel), loaded with AO and analyzed by flow cytometry on 10,000 cells. The fluorescence intensity peak of control cells was set approximately at channel 10^3 and retained for all measurements. Arrowheads indicate the peaks of the lowest red-fluorescent population (here referred to as maximally 'pale' cells) resulting from cells with the most reduced number of intact lysosomes due to LMP. Histograms (lower panel) show the percentage of these pale cells from electronic gating and counting.

Yellow and red bars in the right panel of **Fig. 3A** indicate the number (means ± SD) of autophagosomes and autolysosomes/cell, respectively; the number of cells analyzed for each condition is indicated inside relevant bars; *: $p < 0.002$ (Student's t test). The asterisk in (**B**) indicates a non-specific band. For (**C**) and (**D**) data and significance are as in Fig. 1. **, ***: $p < 0.01$ and $p < 0.001$ *vs* TNF/CHX.

Figure 4. Effect of MT upregulation and ensuing autophagy on TNF/CHX toxicity. (**A**) Cells were exposed to 50 μM $ZnCl_2$ for 24 h. Changes of metallothionein 1A (MT1A) and 2A (MT2A) mRNA levels were measured by real time RT-PCR and presented as relative amounts with respect to untreated cells. (**B**) Cells were exposed for 24 h to the indicated concentrations of $ZnCl_2$ and levels of MT1A mRNA were analyzed by real time RT-PCR and normalized to GAPDH mRNA (upper panel). Equal amounts of proteins from each sample were separated on a 12% denaturing PAGE and transferred to a nitrocellulose membrane for probing with an anti-MT antibody (middle panel).

Loading was assayed by reprobing the membrane with an anti-β-actin antibody (lower panel). (**C**) Cells were treated with $ZnCl_2$ as in (**A**) and starved for different period of times to measure degradation rate of SQSTM1 in the absence or presence of E64d/Leu as in Fig. 3B (representative of three independent experiments). The change in relative amounts of protein at various time points (histograms, right panel) indicates that treatment with 50 μM $ZnCl_2$ to upregulate MTs does not substantially affect autophagic flux. To demonstrate autophagic sequestration of MT (**D-E**) cells were transfected with the plasmids encoding both human MT2A-mCherry and pEGFP-C1-LC3, either left untreated (**D**) or subsequently starved (**E**) in the presence of the various lysosomal inhibitors as indicated. Colocalization is not observed in non-starved cells (**D**), although it is in starved cells, where it is indicated by yellow puncta (**E**, arrowheads). To show lysosomal delivery of autophagocytosed MT (**F-G**), cells were transfected with both hMT2A-GFP and the lysosomal marker LAMP1-mRFP. In unstarved cells (**F**) red and green fluorescence do not overlap. Upon starvation in the presence of various inhibitors of lysosomal degradation (**G**) several enlarged red-labeled, ring-shaped organelles representing lysosomes, which apparently have engulfed some intensely green-fluorescent material, indicate lysosomes containing non-degraded MT2A-GFP (arrows). (**H**) Cells were treated with TNF/CHX following exposure to $ZnCl_2$ for 24 h and ensuing starvation for 2 h. The percentage of apoptotic cells was determined by flow cytometry as in Fig. 1B. (**I**) Maximally pale cells (arrowhead) were detected and quantified as in Fig. 3C. Note almost complete protection in MT-upregulated, starved cells. Numerical data from three independent experiments are presented in the below histograms. For (**H**) and (**I**) 5,000 and 10,000 cells were analyzed for each sample, respectively. The asterisk in (**C**) indicates a non-specific band. Data and statistical significance are as in Fig. 1; §§, §§§; $p < 0.01$ and $p < 0.001$ *vs* controls; ***: $p < 0.001$ *vs* TNF/CHX.

Figure 5. ATG7 silencing abrogates protection from TNF/CHX by MT upregulation and starvation-induced enhanced autophagy. (**A**) Cells were incubated for 72 h with 100 nM siRNA specific for rat

ATG7 and treated with 50 μM $ZnCl_2$ during the last 24 h. ATG7, MT1A and 2A mRNAs were quantified by real time RT-PCR and expressed as relative amounts *vs* cells transfected with non-specific siRNAs. (**B**) The effect of ATG7 silencing on starvation-induced autophagic flux was assayed by transfecting mock- and ATG7-silenced cells with the ptfLC3 construct as described in the legend to Fig. 3A. Quantification of autophagosomes and autolysosomes was performed on single-cell images obtained by confocal microscopy. (**C**) MT was induced with 50 μM $ZnCl_2$ in both control- and ATG7-silenced cells, starved as indicated and exposed to TNF/CHX for another 6 h. Adherent and floating cells were pooled and analyzed by FACS with the annexin V/PI technique. At least 5,000 cells were assayed for each condition. (**D**) Mock- and ATG7-silenced cells were treated with various concentrations of $FeCl_3$, starved and treated with TNF/CHX as described in Fig. 1A. The percentage of pale cells was quantified by FACS as in Fig. 1A.

For panels **A**, **C** and **D** data and statistical analysis of differences are as in Fig. 1; §, §§§: $p < 0.05$ and $p < 0.001$ *vs* control-silenced cells; **, ***: $p < 0.01$ and $p < 0.001$ *vs* TNF/CHX. For panel **B**, yellow and red bars indicate the number (mean ± SD) of autophagosomes and autolysosomes/cell, respectively. The number of cells analyzed for each condition is indicated inside relevant bars; *: $p < 0.005$ (Student's t test).

siControl, siATG7: non-specific and ATG7-specific siRNAs, respectively.

Figure 6. MT silencing abrogates protection from TNF/CHX conferred by MT upregulation. (**A**) Cells were incubated for 72 h with 50 nM siRNAs targeting rat MT1A and 2A (dark and light grey bars, respectively) and treated with 50 μM $ZnCl_2$ during the last 24 h of siRNA treatment. MT1A and 2A mRNAs were quantified by real time RT-PCR and expressed as relative amounts *vs* cells transfected with non-specific siRNAs. The effect of mock and combined MT1A/2A silencing (black and white bars, respectively, **B**), as well as of MT1A alone (**C**) or MT2A alone (**D**) knockdown on protection by $ZnCl_2$ and starvation-induced autophagy against TNF/CHX toxicity was assayed in cells silenced as indicated, treated with $ZnCl_2$ to upregulate MT, starved for 2 h in HBSS/glucose

and eventually exposed to TNF/CHX. Adherent and floating cells were pooled and analyzed by FACS with the annexin V/PI technique. At least 5,000 cells were assayed for each condition. Data and statistical significance are as in Fig. 1; *, **, ***: $p < 0.05$, $p < 0.01$ and $p < 0.001$ *vs* TNF/CHX-treated cells (panels B, **C** and **D**) or mock-silenced cells treated with $ZnCl_2$ (panels **A)**. §§; $p < 0.01$ *vs* cells silenced with siRNAs against both MT1A and 2A and treated with TNF/CHX (panel **B**).

siControl, siMT1A and siMT2A: non-specific, MT1A- and MT2A-specific siRNAs, respectively.

Fig. 1

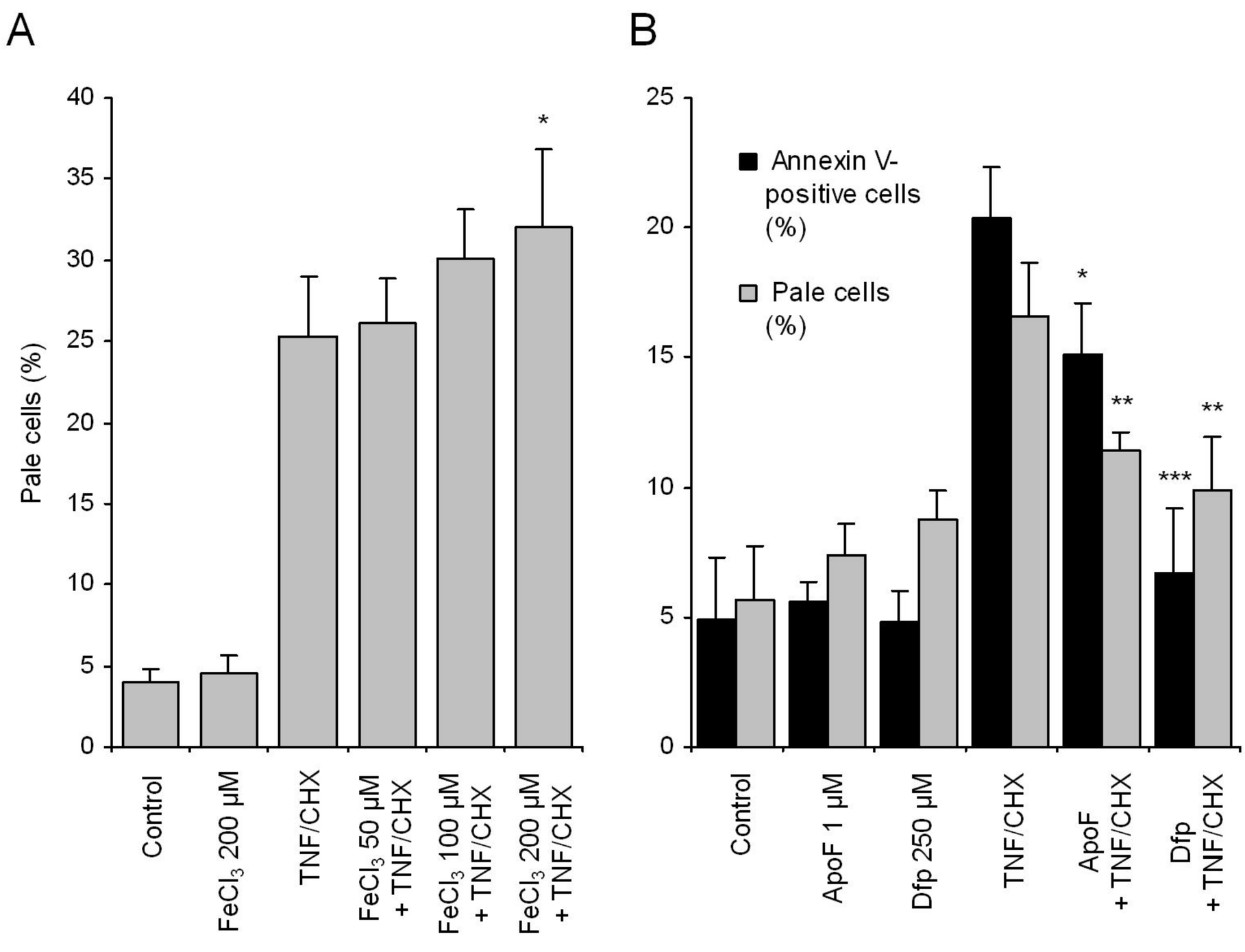
A
Pale cells (%)
40
35
30
25
20
15
10
5
0
*
Control
FeCl3 200 µM
TNF/CHX
FeCl3 50 µM + TNF/CHX
FeCl3 100 µM + TNF/CHX
FeCl3 200 µM + TNF/CHX
B
25
20
15
10
5
0
Annexin V-positive cells (%)
Pale cells (%)
*
**
**
***
Control
ApoF 1 µM
Dfp 250 µM
TNF/CHX
ApoF + TNF/CHX
Dfp + TNF/CHX

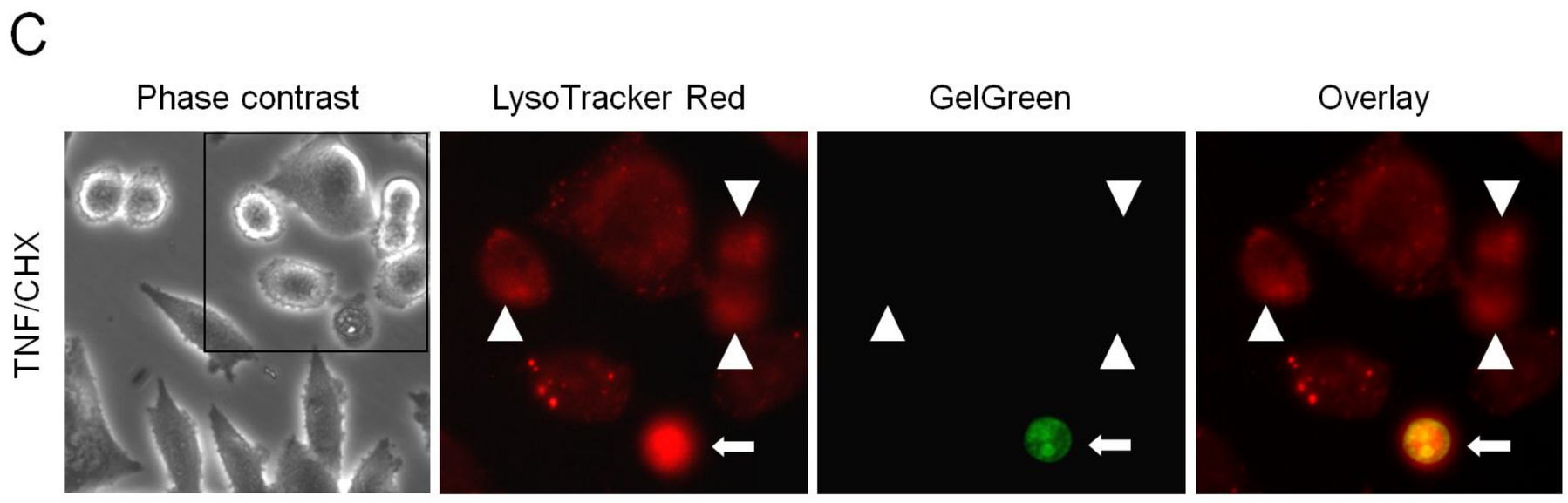
C
Phase contrast
LysoTracker Red
GelGreen
Overlay
TNF/CHX

Fig. 2

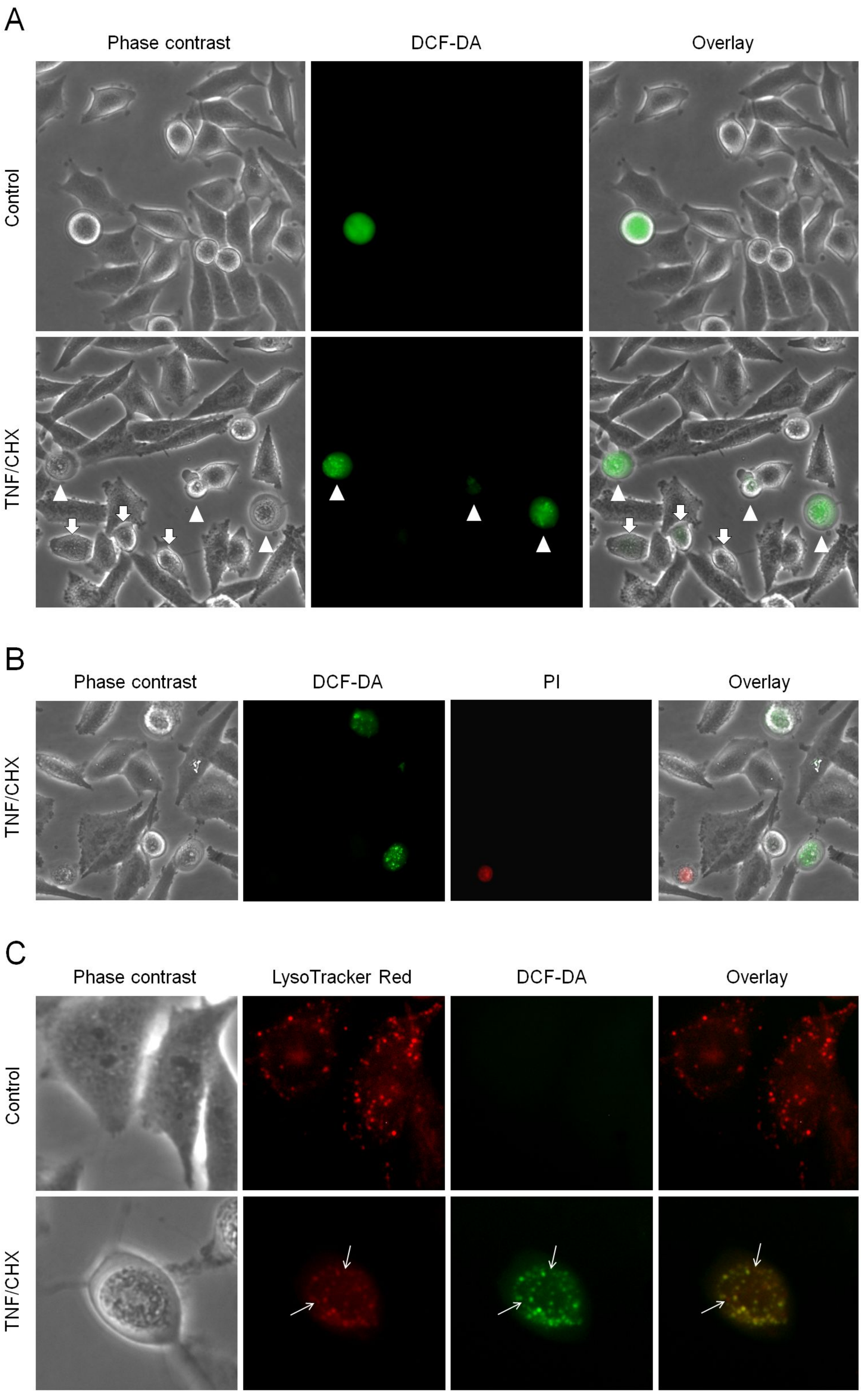
A
Phase contrast
DCF-DA
Overlay
Control
TNF/CHX
B
Phase contrast
DCF-DA
PI
Overlay
TNF/CHX
C
Phase contrast
LysoTracker Red
DCF-DA
Overlay
Control
TNF/CHX

Fig. 3

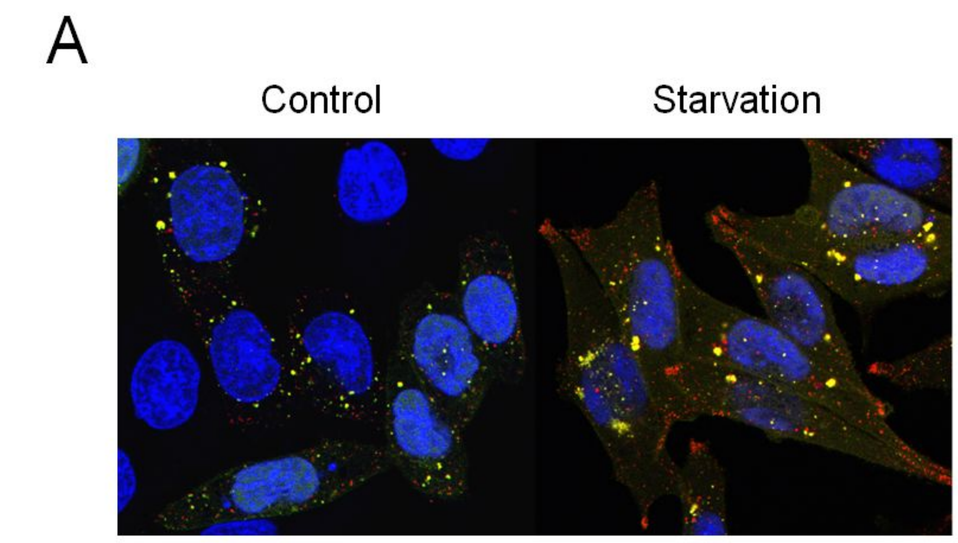
A
Control
Starvation

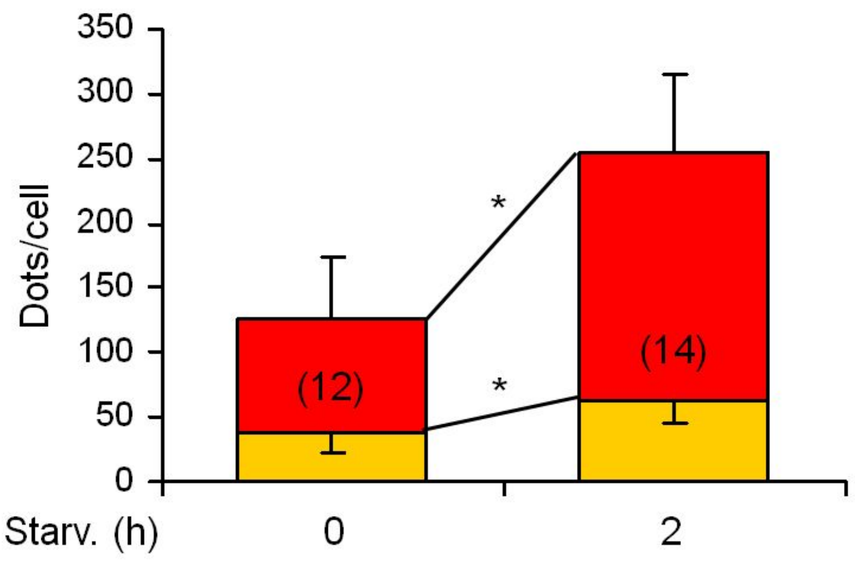
Dots/cell
350
300
250
200
150
100
50
0
(12)
(14)
*
*
Starv. (h) 0 2

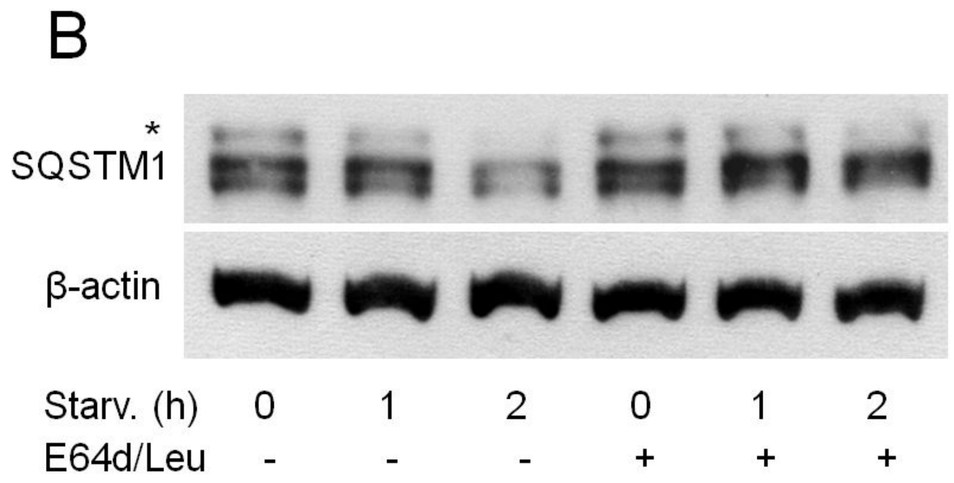
B
*
SQSTM1
β-actin
Starv. (h) 0 1 2 0 1 2
E64d/Leu - - - + + +

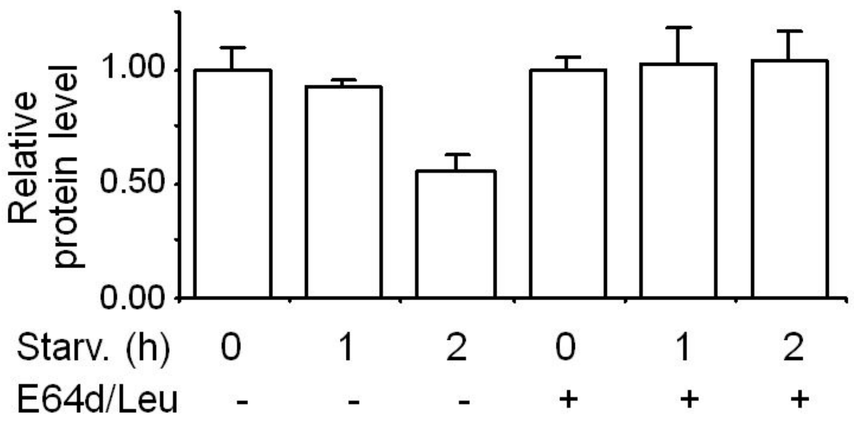
Relative protein level
1.00
0.50
0.00
Starv. (h) 0 1 2 0 1 2
E64d/Leu - - - + + +

C
Annexin V-positive cells (%)
25
20
15
10
5
0
***
***
***
Control
Starv.
NH4Cl
E64d/Leu
TNF/CHX
Starv. + TNF/CHX
NH4Cl + starv. + TNF/CHX
E64d/Leu + starv. + TNF/CHX

D
Cell number
Control
TNF/CHX
Starv. + TNF/CHX
Cell number
Control
TNF/CHX
NH4Cl + TNF/CHX
Red fluorescence
Pale cells (%)
30
25
20
15
10
5
0
**
**
Control
TNF/CHX
Starv. + TNF/CHX
NH4Cl + TNF/CHX

Fig. 4

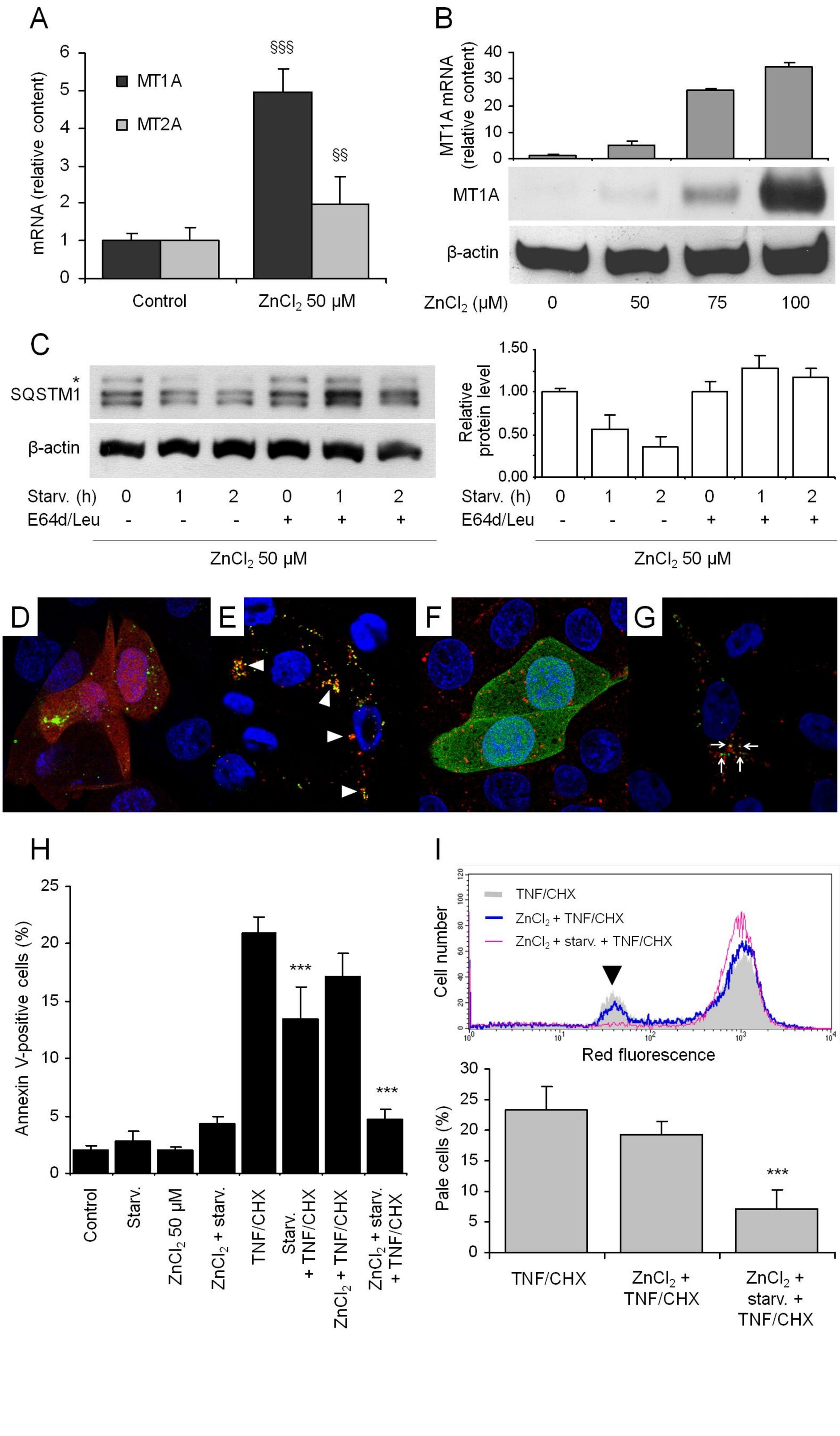
A
mRNA (relative content)
MT1A
MT2A
§§§
§§
Control
ZnCl2 50 μM
B
MT1A mRNA (relative content)
MT1A
β-actin
ZnCl2 (μM) 0 50 75 100
C
SQSTM1*
β-actin
Starv. (h) 0 1 2 0 1 2
E64d/Leu - - - + + +
ZnCl2 50 μM
Relative protein level
Starv. (h) 0 1 2 0 1 2
E64d/Leu - - - + + +
ZnCl2 50 μM
D
E
F
G
H
Annexin V-positive cells (%)
***
***
Control
Starv.
ZnCl2 50 μM
ZnCl2 + starv.
TNF/CHX
Starv. + TNF/CHX
ZnCl2 + TNF/CHX
ZnCl2 + starv. + TNF/CHX
I
TNF/CHX
ZnCl2 + TNF/CHX
ZnCl2 + starv. + TNF/CHX
Cell number
Red fluorescence
Pale cells (%)
***
TNF/CHX
ZnCl2 + TNF/CHX
ZnCl2 + starv. + TNF/CHX

Fig. 5

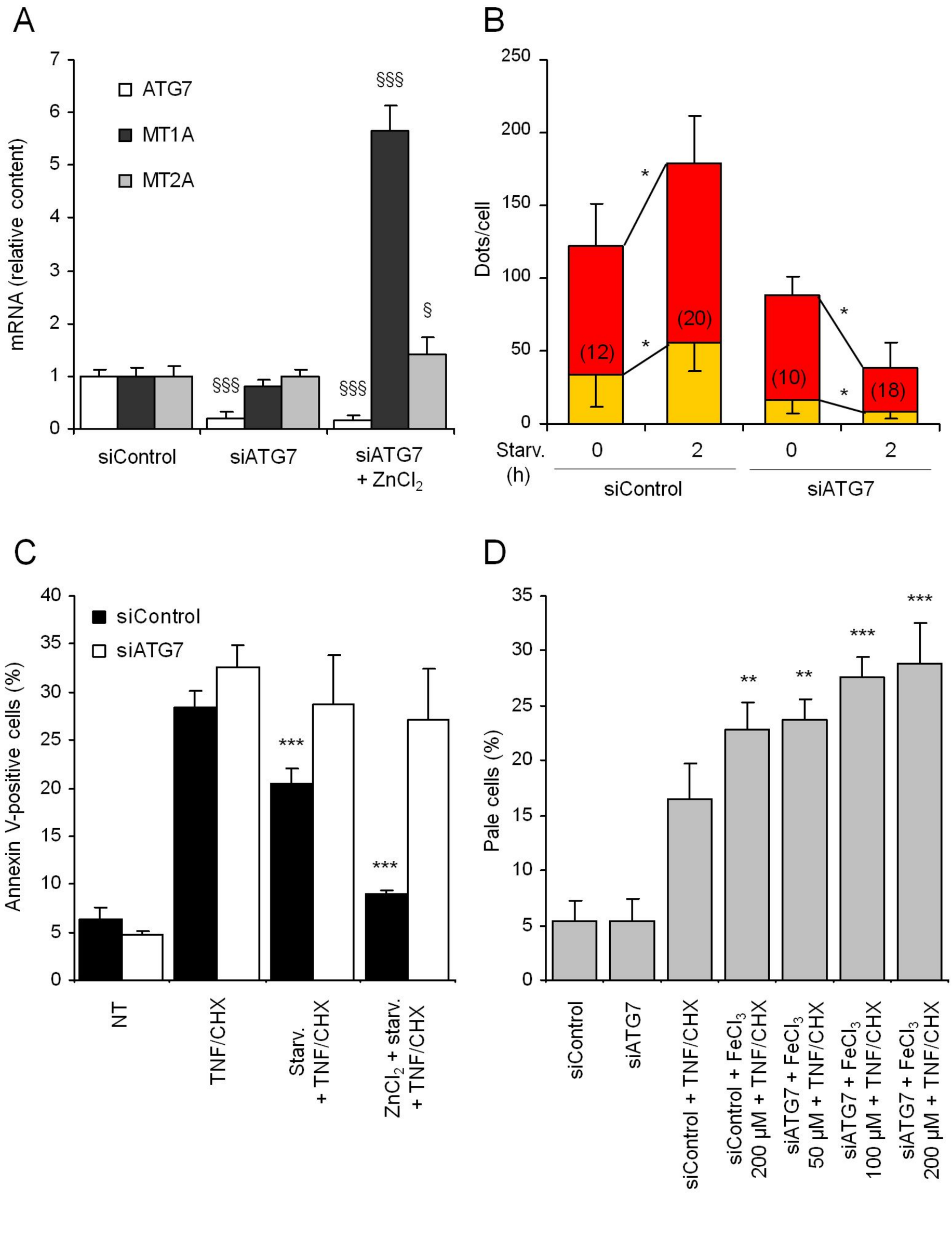
A
mRNA (relative content)
ATG7
MT1A
MT2A
§§§
§
siControl
siATG7
siATG7 + ZnCl2
B
Dots/cell
(12)
(20)
(10)
(18)
Starv. (h)
siControl
siATG7
C
Annexin V-positive cells (%)
siControl
siATG7
NT
TNF/CHX
Starv. + TNF/CHX
ZnCl2 + starv. + TNF/CHX
D
Pale cells (%)
siControl
siATG7
siControl + TNF/CHX
siControl + FeCl3 200 µM + TNF/CHX
siATG7 + FeCl3 50 µM + TNF/CHX
siATG7 + FeCl3 100 µM + TNF/CHX
siATG7 + FeCl3 200 µM + TNF/CHX

Fig. 6

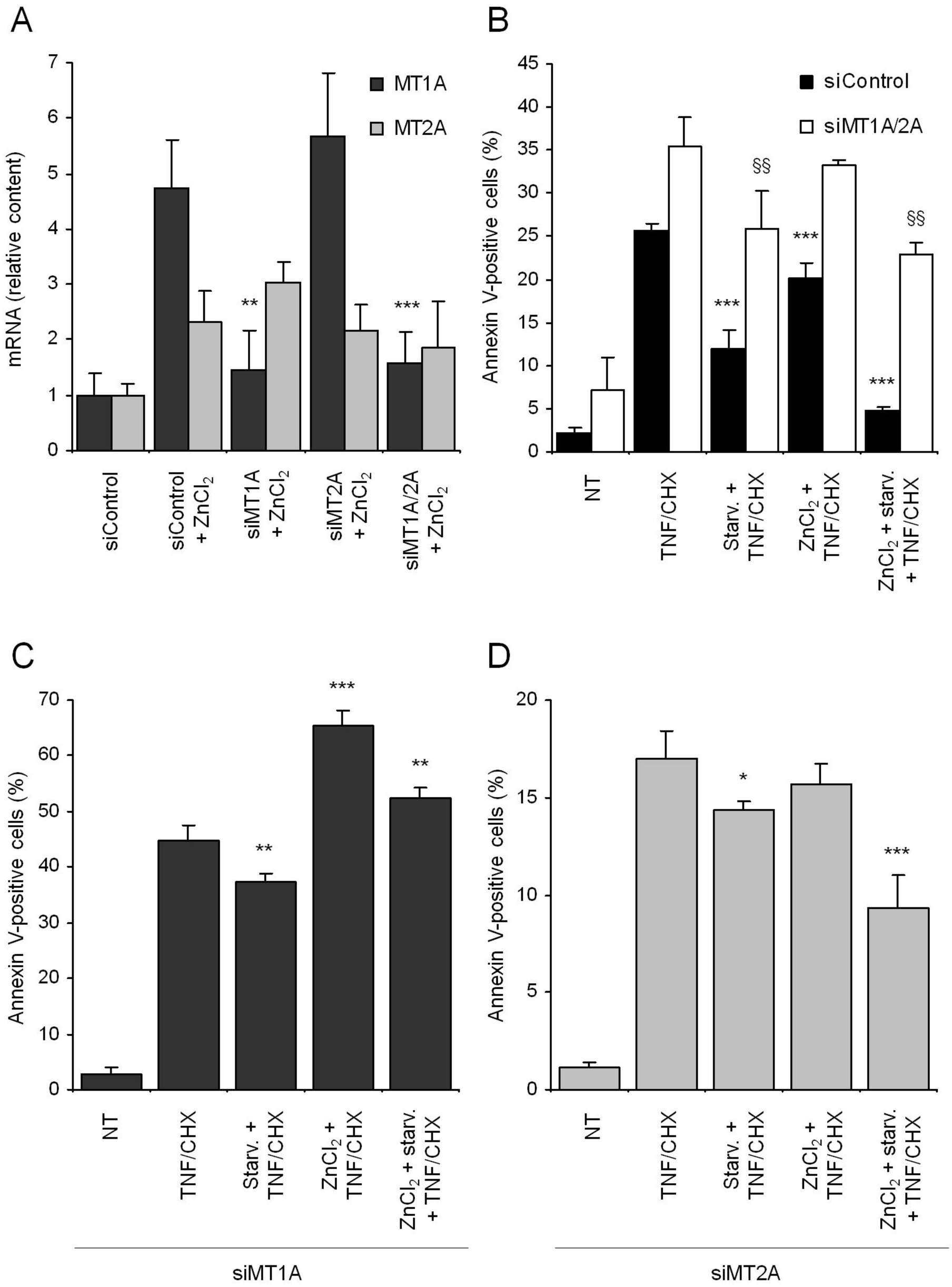
A
B
MT1A
MT2A
siControl
siMT1A/2A
mRNA (relative content)
Annexin V-positive cells (%)
siControl
siControl + ZnCl2
siMT1A + ZnCl2
siMT2A + ZnCl2
siMT1A/2A + ZnCl2
NT
TNF/CHX
Starv. + TNF/CHX
ZnCl2 + TNF/CHX
ZnCl2 + starv. + TNF/CHX
**
***
§§
C
D
Annexin V-positive cells (%)
*
NT
TNF/CHX
Starv. + TNF/CHX
ZnCl2 + TNF/CHX
ZnCl2 + starv. + TNF/CHX
siMT1A
siMT2A

AUTOPHAGY OF METALLOTHIONEINS PREVENTS TNF-INDUCED OXIDATIVE STRESS AND TOXICITY IN HEPATOMA CELLS

Chiara Ullio[1], Ulf T. Brunk[2], Chiara Urani[3], Pasquale Melchioretto[3], Gabriella Bonelli[1], Francesco M. Baccino[1] and Riccardo Autelli[*,1]

[1]Department of Clinical and Biological Sciences, University of Turin, Turin, 10125 Italy;
[2]Division of Pharmacology, Faculty of Health Sciences, Linköping University, Linköping, 58185 Sweden;
[3]Department of Earth and Environmental Sciences, University of Milan Bicocca, Milan, 20126 Italy

Abbreviated title:
Autophagy of metallothioneins prevents TNF toxicity

[*]**Corresponding author:**
Riccardo Autelli Ph.D.
Department of Clinical and Biological Sciences
University of Turin
Corso Raffaello 30
10125 Turin, Italy
Phone: +39 011 6707761
FAX: +39 011 2367761
e-mail: riccardo.autelli@unito.it

Keywords

Autophagy; cell death; hepatoma cells; oxidative stress; iron; lysosomes; TNF.

Abbreviations: AO, acridine orange; ApoF, apoferritin; HBSS, Hank's balanced salt solution; CHX, cycloheximide; DCF-DA, dichlorofluorescein diacetate; Dfp, deferiprone; LMP, lysosomal membrane permeabilization; MT, metallothionein(s); PI, propidium iodide; TNF, tumor necrosis factor; tfLC3, tandem fluorescent microtubule-associated protein 1A/1B-light chain 3-green/red fluorescent proteins chimera; TNFR1 and 2, TNF receptor 1 and 2.

Abstract

Lysosomal membrane permeabilization (LMP) induced by oxidative stress has recently emerged as a prominent mechanism behind TNF cytotoxicity. This pathway relies on diffusion of hydrogen peroxide into lysosomes containing redox-active iron, accumulated by breakdown of iron-containing proteins and subcellular organelles. Upon oxidative lysosomal damage, LMP allows relocation to the cytoplasm of low mass iron and acidic hydrolases that contribute to DNA and mitochondrial damage, resulting in death by apoptosis or necrosis. Here we investigate the role of lysosomes and free iron in death of HTC cells, a rat hepatoma line, exposed to TNF following metallothionein (MT) upregulation. Iron-binding MT does not normally occur in HTC cells in significant amounts.

Intracellular iron chelation attenuates TNF/cycloheximide (CHX)-induced LMP and cell death, demonstrating the critical role of this transition metal in mediating cytokine lethality. MT upregulation, combined with starvation-activated MT autophagy almost completely suppresses TNF/CHX toxicity, while impairment of both autophagy and MT upregulation by silencing of ATG7 and MT1A and/or 2A, respectively,~~of autophagy by ATG7 silencing~~ abrogates protection. Interestingly, MT upregulation by itself has little effect, while stimulated autophagy alone depresses cytokine toxicity to some degree. These results provide evidence that intralysosomal iron-catalyzed redox reactions play a key role in TNF/CHX-induced LMP and toxicity. The finding that chelation of intralysosomal iron achieved by autophagic delivery of MT, and to some degree probably of other iron-binding proteins as well, into the lysosomal compartment is highly protective provides a putative mechanism to explain autophagy-related suppression of death by TNF/CHX.

Word count: ~~228~~241

Introduction

TNF-mediated activation of TNF receptors 1 and 2 (TNFR1; TNFR2) is a powerful inducer of apoptosis/necrosis *in vivo* and *in vitro*. Initially, the death-inducing capability of this cytokine was believed to affect malignant cells only. Later, however, TNF was also found to affect hepatocytes and several other normal cells, and to be active in a number of disorders characterized by cell death and heavy inflammation.[1, 2] The mechanisms by which TNF exerts its effects have been intensely investigated and, at least to some degree, clarified. The TNF-binding capability of TNFR2 was demonstrated more than fifteen years ago,[3] but the full biological role of this receptor remains elusive. It is believed to propagate pro-survival[4] as well as cytotoxic[5] signals, the latter in synergism with TNFR1, which clearly transduces both forms of signals. TNF toxicity was initially accounted for by induction of caspase-dependent apoptotic death,[6] but later alternative non-necrotic, caspase-independent apoptotic-like death mechanisms were reported with increasing frequency.[7, 8]

As ligation of TNF to its two receptors induces both pro- and anti-survival signals, cytotoxicity often becomes less evident, probably as a consequence of NF-kB-dependent upregulation of a number of protective proteins that interfere with cell death programs. TNF toxicity, therefore, may not disclose itself unless the synthesis of such survival factors is restrained.[9-12] It is known that cycloheximide (CHX) and actinomycin D sensitize various cells to TNF, including hepatocytes and hepatoma cells.[13] While most of the known survival factors obstruct caspase-dependent death, others presumably act by different mechanisms. Depending on which death mechanisms TNF triggers, death-suppressing factors may vary substantially.

It is presently well known that the lysosomal compartment is involved in TNF cytotoxicity[14, 15] and that lysosomal membrane permeabilization (LMP) may induce apoptosis/necrosis.[16] Thus, at least some factors protecting against TNF might be proteins that safeguard the stability of lysosomes. Due to their common content of redox-active iron, a result of autophagic degradation of ferruginous materials (such as ferritin and mitochondria), lysosomes are often exposed to iron-

dependent oxidative reactions, including Fenton-type chemistry.[17, 18] These are mainly prevented by limiting the availability of lysosomal free Fe(II). This may occur following autophagy of iron-binding proteins, such as apoferritin, metallothioneins and HSP70, which all suppress LMP caused by oxidative stress.[19-21] The lysosomal presence of low mass labile iron represents a hazard in aerobic cells which produce superoxide and hydrogen peroxide that may diffuse into the lysosomal compartment and initiate Fenton-type reactions.

We previously reported that HTC cells, a rat hepatoma line, are killed by TNF in combination with sub-lethal concentrations of cycloheximide, but are protected by chelation of intracellular redox-reactive iron.[22] More recently, we showed that TNF/CHX-induced death is mediated by LMP.[23, 24] These findings indicate that, indeed, intralysosomal iron, oxidative stress and LMP all contribute to TNF toxicity. In the present study, we further investigate the role of lysosomal iron and LMP following exposure of rat hepatoma cells to TNF/CHX. We show that upregulation of iron-binding metallothionein(s) (MT) in combination with starvation-activated autophagy suppresses TNF toxicity.

Results

Role of iron in LMP and apoptosis-like death of HTC cells by TNF/CHX. In order to find out whether lysosomal iron is important in TNF/CHX-induced death, we exposed HTC cells for 2 h to a precipitate of hydrated iron phosphate, obtained by adding $FeCl_3$ to the medium. The formed insoluble Fe-phosphate is endocytosed and distributes within the lysosomal compartment.[25] While not toxic by itself even at the highest concentration used (200 μM), added iron dose-dependently enhanced TNF/CHX-induced LMP (**Fig. 1A**).

We previously reported that iron chelation by desferrioxamine partly protects HTC cells from TNF/CHX-induced death.[22] In the present work, before TNF/CHX exposure, cells were incubated for 18 h with the low molecular weight, water-soluble, iron chelator deferiprone, or for 4 h with apoferritin. Flow cytometry was used to evaluate both the fraction of annexin V-positive/propidium iodide-negative apoptotic cells and, following exposure to acridine orange (AO), the proportion of 'pale' cells, namely of those exhibiting lower red fluorescence than controls (**Fig. 1B**). This change reflects a reduced number of intact lysosomes, which all display intense red fluorescence, and is a reliable marker of LMP.[26] While apoferritin only partly protected from TNF/CHX-induced death and LMP, deferiprone almost completely prevented both lysosomal alterations and phosphatidylserine externalization in agreement with our earlier reports.[22] In our system, moderate LMP was an early and asynchronous event distinct from necrosis and associated with moderate cell shrinkage. Cells showing low to moderate LMP retained plasma membrane integrity and did not take up the GelGreen dye (**Fig. 1C**, arrowheads), indicating that necrosis is not yet occurring at this stage. By contrast, highly condensed cells, showing diffuse LysoTracker Red staining (necrotic cells), also displayed intense green fluorescence (**Fig. 1C**, arrow). These data are in good agreement with our previous results and those of other groups and support the view that LMP is a major effector mechanisms of TNF/CHX-induced death, and not a mere consequence of death itself.

Involvement of lysosomes in TNF/CHX-induced alterations of intracellular redox homeostasis. As the presented results strongly suggest that iron actively mediates TNF/CHX-induced cell death, the redox status of cytokine-treated HTC cells was evaluated by means of dichlorofluorescein diacetate (DCF-DA). This ester freely permeates the plasma membrane; in the cytoplasm it is split by non-specific esterases to yield a non-membrane permeable alcohol (DCF), which turns highly green-fluorescent if oxidized by hydroxyl radicals or peroxidase reactions.[27] In controls, only a few cells (**Fig. 2A**, upper panels) appeared rounded up and showed intense fluorescence, probably representing dying cells in which Fenton-like reactions occur owing to relocation of redox-active iron from bursting lysosomes to the cytoplasm in combination with production of hydrogen peroxide from damaged mitochondria. TNF/CHX markedly affected the morphology of cells, some of which exhibited either intense or low green fluorescence (**Fig. 2A**, lower panels, arrowheads and arrows, respectively), confirming that the cellular redox status was altered by TNF/CHX. Interestingly, many of these cells displayed a characteristic punctate fluorescence, yet not all cells undergoing morphological alterations stained positive for DCF, presumably indicating that redox perturbations occurred asynchronously in the population, as already observed for LMP (see **Fig. 1C**). Cells displaying such a punctate pattern of DCF positivity were moderately shrunk, but clearly not yet necrotic as they still effectively excluded PI (**Fig. 2B**). The latter dye, however, freely permeated the highly condensed cells, which also were totally devoid of granular DCF fluorescence. TNF/CHX-induced granular DCF fluorescence markedly differed from that generated by H_2O_2, used as a positive control to induce oxidative stress, in which a strong and diffuse DCF fluorescence was observed, with no evidence of any punctate pattern (not shown). This difference suggests that, in TNF/CHX-treated cells, the outbreak of oxidative stress was initiated in specific areas of the cytoplasm. Coupled with the requirement of a functional acidic compartment for TNF/CHX toxicity,[22] this finding suggested that the fluorescent dots highlighted by DCF might be lysosomes. To clarify this point, cells treated with TNF/CHX were subsequently

stained with both DCF-DA and LysoTracker Red, a fluorescent probe for the lysosomal compartment. Only red fluorescence identifying intact lysosomes was detectable in control cells, with no positivity for DCF (**Fig. 2C**, upper panels). By contrast, in TNF/CHX-treated cells many LysoTracker-positive dots (lysosomes) were also positive for DCF, thus appearing yellowish in overlays (**Fig. 2C**, lower panels). This observation confirms that the lysosomal compartment was engaged in an intense redox activity consequent to treatment with TNF/CHX. Of interest, a few red-stained lysosomes were invisible when viewed under blue light to detect the green fluorescence of oxidized DCF (**Fig. 2C**, lower panels, white arrows), indicating that no oxidative reactions took place in those organelles. This suggests that TNF/CHX do not uniformly affect all lysosomes and that the co-staining may be a consequence of early and partial permeabilization of the membrane of particularly iron-rich lysosomes allowing the hydrophilic alcohol DCF to enter before lysosomal stability is completely lost.

Effects of starvation-enhanced autophagy on TNF/CHX toxicity. To analyze the role of autophagy on TNF toxicity, cells were starved by incubation in Hank's balanced salt solution (HBSS) for 2 h before being exposed to TNF/CHX. Starvation markedly stimulated autophagic flux, as demonstrated by increased number of autophagosomes and autolysosomes/cell (yellow and red puncta, respectively; **Fig. 3A**), and the degradation of SQSTM1/p62 (**Fig. 3B**), which was totally abrogated by a mixture of the lysosomal cathepsins B, H and L inhibitors E-64-d/leupeptin. Starvation-induced autophagy reduced TNF/CHX toxicity by about 40% (**Fig. 3C**), suggesting that some autophagocytosed cytoplasmic factors interfere with death signals triggered by TNF/CHX. Should this be the case, preventing intralysosomal degradation of autophagocytosed material would be expected to enhance starvation-associated protection. To test this possibility, starvation was performed in the presence of NH_4Cl in order to impair lysosomal degradation without affecting the early stages of the autophagic process.[28] As expected, NH_4Cl further increased the protection conferred by starvation (**Fig. 3C**) and, though reducing the staining of cells with intact lysosomes,

markedly diminished the frequency of pale cells independently of concomitant starvation, thus confirming that inhibiting lysosomal degradation significantly affects ~~activity is required for~~ TNF/CHX toxicity ~~to occur~~ (**Fig. 3D**). Similar results were obtained when acidic proteolysis was blocked by bafilomycin A1, a specific V-ATPase inhibitor that prevents lysosomal acidification (not shown). To confirm that the effect of NH_4Cl actually relies on impairment of lysosomal degradative activity, and not merely on their alkalinization, an E-64-d/leupeptin mixture was added simultaneously with starvation to selectively block acidic proteolysis. In keeping with NH_4Cl, the cathepsin inhibitors potentiated starvation-induced protection from TNF/CHX (**Fig. 3C**), thus supporting the view that blocking lysosomal degradation of autophagocytosed materials increases protection from death achieved by starvation-induced autophagy.

This finding strongly suggests that enforced autophagy and impaired intralysosomal degradation of autophagocytosed materials interfere with the propagation of TNF/CHX-related death signals.

Effect of metallothionein (MT) autophagy on TNF/CHX toxicity. The above findings suggest that starvation promotes the sequestration of iron-chelating proteins from cytoplasm into the lysosomal system. Since MT upregulation has been reported to protect against LMP induced by various kinds of oxidative stress,[29] we focused on this group of proteins, which bind a variety of metals, including iron [for a review see[30]] and, particularly, on the inducible 1A and 2A isoforms. The latter, in particular, are scarce in HTC cells and, therefore, upregulation of such proteins represents a suitable model to verify whether autophagy of iron-binding proteins may protect lysosomes and cells against oxidative stress. To test this hypothesis, we upregulated MTs by adding 50 μM $ZnCl_2$ to the growth medium for 24 h before ensuing starvation (or not) for 2 h and final treatment with TNF/CHX for 6 h. Exposure to $ZnCl_2$ increased the amount of both MT mRNAs (**Fig. 4A**), the 1A form markedly more than 2A (5 and 2 folds, respectively). The response of MT1A mRNA and protein to $ZnCl_2$ in the range of 50 - 100 μM was dose-dependent (**Fig. 4B**). Of

interest, 50 μM $ZnCl_2$ affected neither the starvation-induced degradation of SQSTM1, nor its prevention by E-64-d/leupeptin. This indicates that neither autophagy nor lysosomal proteolysis was affected by $ZnCl_2$ treatment (**Fig. 4C**). We next investigated whether, following starvation, upregulated MT is actually autophagocytosed and transferred to lysosomes. To this purpose, a plasmid encoding human MT2A-GFP was transfected together with a reliable autophagosomal marker.[31] Cells were then left untreated (**Fig. 4D**) or starved for 2 h as described (**Fig. 4E**), permeabilized with digitonin[32] and imaged using a confocal microscope. In controls, red fluorescence resulting from hMT2A-mCherry was dispersed all over the optical section, indicating no specific colocalization of this protein with the autophagosomes (green-fluorescent, due to LC3-GFP). Starvation brought about the formation of several cytoplasmic clusters of yellow dots (**Fig. 4E**, arrowheads), indicating colocalization (43.13 ± 4.3 % colocalization, as compared to 1.8 ± 2.5 % for controls) of hMT2A and the autophagosomal marker in identical regions of the analyzed optical sections. Such a colocalization, therefore, demonstrates that hMT2A is actually autophagocytosed by HTC cells following starvation.

To further investigate whether autophagic flux stimulated by starvation may allow the transfer of MT from autophagosomes to lysosomes, cells were transfected with both MT2A-GFP and the lysosomal marker LAMP1-mRFP, either left untreated (**Fig. 4F**) or starved for 2 h as described (**Fig. 4G**). In control cells, the green fluorescence of MT2A-GFP was evenly widespread all over the focal plan and unrelated to the LAMP1-mRFP signal, which, as expected, clustered in discrete red dots representing lysosomes. Starvation in the presence of lysosomal inhibitors gave rise to several red-fluorescent organelles (**Fig. 4G**, arrows), with an intensely green-fluorescent content, indicating the presence of MT2A. As MT was found to be autophagocytosed following starvation (**Fig. 4E**), its association to large vesicular LAMP1-positive organelles (28.7 ± 10. 1 % colocalization, compared to 0 % for non-starved cells) suggests that enlarged lysosomes, deriving from the blockade of acidic proteolysis by the used lysosomal inhibitors, also carry a significant

amount of MT2A-GFP chimera. This finding thus confirms that starvation-induced autophagic sequestration of MT actually takes place and precedes its subsequent delivery to lysosomes.

Eventually, the biological effect of MT upregulation and autophagy on TNF/CHX toxicity was investigated. Even minor MT upregulation, such as that achieved by the lowest $ZnCl_2$ concentration used, slightly attenuated TNF/CHX toxicity and LMP (**Fig. 4H** and **I**, respectively). Protection associated with MT upregulation alone was somewhat lower than that achieved by starvation alone (**Fig. 4H**). However, when starvation-enhanced autophagy followed MT induction, it became nearly complete, indicating that TNF toxicity is almost fully abrogated by starvation-induced autophagy of previously upregulated metallothioneins.

The relevance of autophagy in suppressing TNF toxicity was further investigated by transiently silencing ATG7, a protein essential in triggering this process.[16] siRNA effectively decreased the amount of ATG7 mRNA, but not that encoding for MT1A and 2A. Also MT upregulation by 50 μM $ZnCl_2$, which increased MT1A and 2A mRNAs by about 5.5 and 1.5 folds, respectively, was totally unaffected by silencing (**Fig. 5A**). ATG7 silencing, however, markedly impaired starvation-induced autophagic flux as evidenced by the markedly depressed number of autophagosomes and autolysosomes/cell formed following 2 h of starvation (**Fig. 5B**). As expected, impaired autophagy consequent to ATG7 silencing abrogated the protection from TNF toxicity conferred by starvation, either alone or following MT upregulation (**Fig. 5C**). We ~~eventually~~ also investigated whether autophagy plays any role in Fe-induced sensitization to TNF (see **Fig. 1A**). To this aim, mock- and ATG7-silenced cells were treated with TNF/CHX in the presence of increasing amounts of unsoluble $FeCl_3$. Extensively pale cells were then quantified by flow cytometry. ATG7 silencing did not substantially modify the capability of Fe to sensitize HTC cells to TNF/CHX-induced LMP ~~toxicity~~ (**Fig. 5D**). This result~~,~~ thus indicates~~ing~~ that ~~basal~~ inhibition of autophagy does not interfere with ~~play any relevant role in Fe induced~~ sensitization to TNF/CHX ~~mediated by~~due to endocytosis of the Fe-phosphate complex.

Eventually, the specific role of MTs in $ZnCl_2$-related protection of HTC against TNF/CHX was investigated by interfering with upregulation of either MT1A or 2A, or of both simultaneously, by siRNA application before starvation and exposure to TNF/CHX. While a scrambled siRNA did not affect MT induction by $ZnCl_2$, MT1A- and MT2A-specific siRNAs effectively prevented MT upregulation, in particular when MT1A was affected (**Fig. 6A**). When silenced cells were subsequently exposed to TNF/CHX with or without starvation, siControl did not affect the overall response to the cytokine (**Fig. 6B**, black bars) with respect to non-silenced cells (as shown in **Fig. 4H**). By contrast, siRNAs targeting MT1A or MT2A, both combined (**Fig. 6B**, white bars) and separately (**Fig. 6C** and **D**, respectively) totally abrogated $ZnCl_2$-induced protection. Remarkably MT1A silencing increased susceptibility of HTC cells to TNF/CHX more markedly than MT2A silencing, suggesting a minor role for MT2A in protecting these cells against cytokine toxicity. Of interest, MT silencing, while effectively eradicating protection by $ZnCl_2$, did not affect that conferred by autophagy, probably due to persistent sequestration and lysosomal delivery of normally available cytoplasmic iron-binding proteins other than MT(s). These results, combined with those in which autophagy was restrained by ATG7 silencing, thus definitely support our hypothesis that lysosomal delivery of upregulated MT is the key mechanism by which autophagy protects HTC cells against TNF/CHX-induced death.

Discussion

Cell death is frequently, though not invariably, observed in eukaryotic cells exposed to TNF. Interestingly, the toxic effect often only occurs, or is at least much more pronounced when the cytokine is combined with inhibition of macromolecular synthesis.[33] Depending on cell type, TNF triggers either caspase-dependent or -independent death pathways [reviewed in[6, 34]]. Although caspase activation, as part of extrinsic or intrinsic apoptotic pathways, was earlier considered primarily responsible for TNF-induced death(s), accumulating evidences now suggest that in a number of cases TNF toxicity is independent from, yet possibly occurring together with, caspase activation.[13, 35, 36] Among caspase-independent deaths, mechanisms such as induction of oxidative stress and release of acidic proteases from lysosomes have been reported to play a significant role in TNF toxicity *in vivo* and *in vitro*.[2, 37-39] So far, the exact mechanisms by which TNF triggers oxidative stress and affects cells and organelles remain elusive.

We previously reported that TNF/CHX trigger apoptotic-like death in rat hepatoma cells that are significantly protected by drugs that raise lysosomal pH, by the iron chelator desferrioxamine and lipophilic antioxidants as well as by NADPH oxidase inhibitors.[22] Collectively, these findings suggest that intralysosomal iron and NADPH oxidase are major mediators of TNF toxicity, pointing to a prominent role of redox-centered reactions in TNF/CHX-induced death of hepatoma cells.

In the present study, we further demonstrate that TNF/CHX-induced LMP and ensuing cell death are slightly but significantly increased by incubating HTC cells in the presence of an iron-phosphate complex that is endocytosed and split in the acidic lysosomes, thereby increasing their content of low-mass, redox-active iron. By contrast, they are markedly attenuated by iron chelators such as deferiprone or apoferritin, both more effective than desferrioxamine that does not readily cross the plasma membrane but is taken up by endocytosis.[40] Iron availability thus appears critical in influencing HTC death, strongly supporting the notion that it plays a central role in TNF/CHX toxicity. Low-mass iron is well known to be physiologically available in lysosomes, mainly

deriving from the breakdown of autophagocytosed ferruginous materials,[25, 41] such as ferritin and mitochondria that carry the major share of intracellular iron.[42] Upon degradation of the protein backbone, bound iron is freed in the lysosomal lumen and kept in ferrous (Fe^{2+}) form by the low pH and the reducing environment of lysosomes.[17, 43] Its redox-reactive configuration makes intralysosomal iron very prone to participate in Fenton-like reactions in the presence of H_2O_2. In this context, iron chelation acts as a chain-breaking event that prevents initiation of harmful redox reactions. Many studies have convincingly demonstrated that iron chelation affords protection in a number of oxidative stress-based models of cell death.[44] This scenario seems plausible in this model as well, and is fully supported by our previous demonstration that diphenylene iodonium, a putative inhibitor of NADPH oxidase, disrupts TNF/CHX toxicity.[22] TNF is known to activate NADPH oxidase in different cell types.[45, 46] In professional phagocytes its presence in plasma- and lysosomal membranes[47] is reported to account for intralysosomal Fenton-type reactions.[44] Superoxide produced by NADPH oxidase, inside or outside the lysosomal compartment, is rapidly dismutated to hydrogen peroxide that in turn would react with lysosomal free Fe^{2+}. If extensive, the oxidative process might propagate to the lysosomal membrane, where lipid peroxidation results in LMP and release of lysosomal contents, namely acidic hydrolases and low mass redox-active iron, into the cytoplasm.[48] Simultaneous staining by DCF and LysoTracker Red indicates that many, but not all lysosomes undergo a burst of oxidative reactions, which likely account for LMP. Importantly, this finding shows that lysosomes are differently sensitive to oxidation, probably because of different contents or redox-active iron.[19, 49] Lysosomal retention of LysoTracker Red for some time after initiation of oxidative stress witnesses that pronounced LMP is not an early event. Initially, only partial LMP seems to occur, allowing hydrophilic DCF to enter some lysosomes, but also LysoTracker Red to remain intralysosomally, while the plasma membrane is still intact. Further progress of LMP allows the release of lysosomal contents to the cytoplasm, contributing to the complete loss of selective plasma membrane permeability.

The results suggest that, at least in HTC cells, intralysosomal oxidative activity is an early event during cellular response to TNF/CHX. The retention in many lysosomes of LysoTracker Red early in the apoptotic cascade indicates that lysosomal membranes are not yet fully permeabilized. Of interest, our data also show that, simultaneously, some lysosomes do not allow DCF to enter. The most likely explanation for this lysosomal heterogeneity, which has been pointed out before,[49] is that, within a given population, lysosomes may largely differ with respect to their content of iron. Based on the above considerations, it was highly expected that chelation of endo-lysosomal, redox-active iron would provide good protection against TNF/CHX.

In agreement with a number of reports showing that autophagy protects from oxidative damage,[50-52] starvation-enhanced autophagy significantly attenuated HTC cell death by TNF/CHX, while ATG7 silencing prevented this effect. These findings strongly suggest that an altered iron/iron chelator balance within lysosomes, for example due to increased autophagy of available Fe-binding proteins, probably mainly ferritin, might account for this effect. This hypothesis was strengthened by the observation that NH_4Cl and selective cathepsin inhibitors both markedly potentiated protection from death by delaying lysosomal breakdown of autophagocytosed iron-chelating proteins (by lysosomal alkalinization and cathepsin inhibition) and allowing time for expelling most low-mass iron from the lysosomal compartment. To further prove our hypothesis we upregulated cytoplasmic MTs, normally expressed to very low levels in HTC, by exposing them to zinc prior to starvation. MTs are a class of low-abundance cytoplasmic SH-rich proteins binding a variety of metals, iron included,[30] whose upregulation has been shown to be highly protective against a number of harmful conditions, in particular those in which oxidative stress is involved.[29, 53-57] These proteins are often overexpressed in various cancers, making them more resistant to irradiation and drugs that induce oxidative stress.[58] In the present work, MT1A and 2A were found poorly expressed in HTC cells under basal conditions, but were easily upregulated by $ZnCl_2$. We also provide evidence that transiently overexpressed MT2A-GFP is sequestered in autophagosomes during starvation-induced autophagy and that some of it eventually relocalizes to lysosomes. Thus,

autophagic flux actually redirects cytoplasmic MTs to the lysosomal compartment, where they will chelate intralysosomal redox-active iron, suppress LMP and protect cells from TNF/CHX-induced death. In agreement with these results, selective targeting of this protective mechanism, namely MT upregulation and their autophagy-mediated relocation to the acidic compartment, significantly restrain resistance of HTC to TNF/CHX toxicity. As expected, MT1A and 2A silencing abrogated protection afforded by Zn, while that due to starvation alone was mainly unaffected. In keeping with the above results, we further provide evidence that ATG7 -silencing counteracted the almost full protection brought about by starvation-enhanced autophagy of MT. Interestingly, in rat liver, degradation of this class of iron-binding proteins is accounted for mostly by the lysosomal cathepsins B and L.[59, 60] Consequently, inhibition of lysosomal proteolysis achieved by either NH_4Cl or the cathepsins B and L inhibitors E-64-d/leupeptin potentiated protection brought about by starvation, presumably by slowing down lysosomal degradation of autophagocytosed MTs. Of interest, the lowest zinc concentration used only weakly upregulated MTs and by itself only slightly protected from death, yet in combination with starvation-induced autophagy gave rise to a nearly total protection against TNF/CHX. This observation demonstrates that coupling upregulation of iron-binding proteins with autophagy is needed to disrupt the redox events that lead to LMP and death.

Collectively, the present results demonstrate that MT upregulation in combination with its enforced autophagic relocation to the lysosomal compartment is very effective in protecting HTC cells from the toxic effects of TNF/CHX. Therefore, the results also demonstrate that lysosomal iron-centered redox reactions largely account for TNF/CHX-induced LMP and toxicity and that oxidative stress is a major mechanism of TNF toxicity in HTC hepatoma cells.

Materials and Methods

Cell cultures and treatments. The HTC, a rat hepatoma cell line, were grown in a 1:1 mixture of DMEM/Ham's F12 medium (Sigma-Aldrich, D6421) supplemented with 10% FBS (Gibco, 10270106), 2 mM glutamine (Sigma-Aldrich, G3126), 100 U/ml penicillin and 100 µg/ml streptomycin (Sigma-Aldrich, P4333) in 95% humidified air with 5% CO_2. For experiments, cells were seeded at 10^4 cells/cm^2 and 18 h later exposed to 20 ng/ml TNF (R&D Systems, Minneapolis, 210-TA) plus 10 µg/ml CHX (Sigma-Aldrich, C7698) for 6 h. For MT upregulation, cells were incubated for 24 h with various concentrations of $ZnCl_2$ (Sigma-Aldrich, 429430). Autophagy was stimulated by starvation for 2 h in HBSS supplemented with 0.31% glucose at 37 °C, after which they were returned to standard growth conditions and further treated as above. Deferiprone and apoferritin (Sigma-Aldrich, 379409 and A3660, respectively) were dissolved in growth medium and added at the indicated concentrations 18 and 4 h before TNF/CHX treatment, respectively.

Quantification of MT1A, -2A and ATG7 mRNAs by real time RT-PCR. To evaluate the levels of the above transcripts, total RNA was extracted with the TriPure Isolation Reagent (Roche Diagnostics, 11667157001); 1 µg total RNA was reverse-transcribed in a 20 µl reaction using the Reverse Transcription System (Promega, A3500). Real time PCR was performed on 50 ng cDNA using the iQ SYBR Green Supermix (BioRad Laboratories, 170-8880) and an iCycler. Primers used (forward and reverse primer) were: MT1A: 5'-CCAACTGCTCCTGCTCCAC-3' and 5'-GAGGCACCTTTGCAGACACA-3'; MT2A: 5'-ATGGACCCCAACTGCTCCT-3' and 5'-GCACTTGTCCGAAGCCTCTT-3'; ATG7: 5'-ACCCTGCACAACACCAACAC-3' and 5'-GAGCATGGGGTTTTCGAGAG-3'. Normalization was performed with respect to the total amount of rat GAPDH mRNA for each sample as detected with the following primers: 5'-CCACTCAGAAGACTGTGGATGG-3' and 5'-GGATACATTGGGGGTAGGAACA-3'. The relative change of mRNAs under the various conditions was calculated using the $2^{-\Delta\Delta C_T}$ method.

Determination of autophagic flux. The effect of starvation on autophagic flux was assayed by transfecting the cells with the ptfLC3 plasmid[61] (Addgene plasmid 21074). Cells were plated at 8 x 10^3 cells/cm^2 onto a μ-Slide VI (Ibidi GmbH, 80606) and transfected 18 h later with 2 μg of the plasmid with Lipofectamine 2000 (Invitrogen, 11668-019). About 30 μl of DNA complex was added to each channel of the μ-Slide in antibiotic-free medium for 24 h to both control and ATG7-silenced cells. The next morning, cells were washed twice with PBS and returned to standard culture conditions for another 24 h before being starved as described above. Following starvation, cells were rinsed once with PBS, fixed for 20 min with 4% formaldehyde and rinsed twice with PBS before confocal examination. Samples were analyzed with a Leica TCS SP5-AOBS 5-channel confocal system (Leica Microsystems) equipped with a 405-nm diode, an argon ion, a 561-nm DPSS, and a 633-nm HeNe laser. Images were acquired using a HCX PL APO 63x/1.4 NA oil immersion objective at a pixel resolution of 240 x 240 or 80 x 80 nm and further processed with Photoshop 7.0. In order to make counting of autophagosomes and autolysosomes (yellow and red fluorescent dots, respectively) reliable and basically independent of the operator,[62] the Green and Red Puncta Colocalization ImageJ Plugin (created by Daniel J. Shiwarski, University of Pittsburgh; enhanced and modified by Ruben K. Dagda, University of Nevada School of Medicine and co-approved as an image tool for autophagic flux by Charleen T. Chu, University of Pittsburgh), was used without any setting change or adjustment on a number (indicated in each relevant histogram) of single-cell images extracted from different microscopic fields (3 to 6 for each experimental condition).[63]

Autophagy and lysosomal delivery of MT. For detection of MT autophagy, a construct (pcDNA3-hMT2A-mCherry) encoding a human MT2A-mCherry was generated by ligase-independent cloning of the MT2A cDNA (PCR-amplified from pcDNA3-GFP-hMT2A; Addgene plasmid 11613) into the pcDNA3-mCherry LIC cloning vector (6B) (Addgene plasmid 30125). pcDNA3-hMT2A-mCherry was cotransfected with the autophagosomal marker pEGFP-C1-LC3. For analysis of

lysosomal delivery of MT, the pcDNA3-GFP-hMT2A was cotransfected with the lysosomal marker pLJM1-LAMP1-mRFP-FLAG (Addgene plasmid 34611).

For transfections, cells were seeded at the density of 3 x 10^3/cm^2 in individual wells of µ-Slides 8 wells (Ibidi GmbH, 80826, ibiTreat) and transfected 24 h later with 0.4 µg of the above constructs with Lipofectamine 2000 in antibiotics-free medium (DNA:Lipofectamine 2000 ratio of 1:0.75). The next morning cells were returned to complete growth medium for an additional period of 24 h. Cells were then pretreated with 100 µM E-64-d (Santa Cruz Biotechnology, sc-201280) plus 10 µM leupeptin (Enzo Life Science, ALX-260-009) for 60 min, after which they were starved for 2 h in HBSS/glucose in the presence of the above inhibitors plus 1 µM bafilomycin A1 (Adipogen, BVT-0252), added to the starvation medium without any pretreatment. During starvation, cells were stained for 60 min with 0.5 µg/ml Hoechst 33258 (Sigma-Aldrich, 861405). Before fixation, cells were permeabilized for about 1 (controls) or 2-3 (starved cells) min with 100 µg/ml digitonin in PBS (Sigma-Aldrich, D5628) at room temperature. This method is a modification of the original saponin-based technique.[32] The setting of permeabilization conditions was performed by monitoring the increase of red fluorescence following incubation of cells for 2 min with increasing concentrations of digitonin in the presence of 20 µg/ml of propidium iodide (Sigma-Aldrich, P4170). A concentration of 100 µg/ml digitonin was chosen as it resulted in a positivity of more than 95% cells to PI as evaluated by FACS analysis (not shown). Shorter permeabilization of controls was required in order to show the expression of transfected hMT2A, using either the -mCherry or -GFP variant, as a longer permeabilization totally released the protein not segregated inside the autophagosomes or lysosomes by starvation. After permeabilization, cells were fixed with 4% formaldehyde for 20 min and stored for confocal analysis; recorded images were composed with Photoshop 7.0 as described above.

Colocalization analysis was performed with the JACoP[64] tool for ImageJ (using the 'object-based' method) on at least 5 single cells extracted from independent microscopic fields.

Detection of lysosomal oxidative activity. For detection of oxidative stress, cells were treated with TNF/CHX as above, or with 10 mM H_2O_2 (initial concentration; Sigma-Aldrich, H1009) for 30 min in PBS as a positive control, followed by another 5.5 h recovery in complete growth medium under standard culture conditions. Cells were then loaded with 10 μM dichlorofluorescein diacetate (DCF-DA; Sigma-Aldrich, D6883) for 30 min, in growth medium without phenol red. When simultaneous detection of the lysosomal compartment was required, 25 nM LysoTracker Red was added 10 min after start of staining with DCF-DA. Cells were then exposed to both tracers for another 10 min. Total DCF-DA loading time was thus shortened to 20 min to increase the ratio of puncta to cytoplasm staining. Residual dye was removed by a medium change. Following addition of fresh growth medium, cultures were promptly imaged using an inverted fluorescence microscope and representative pictures acquired and composed as described above.

Flow cytometric quantification of apoptosis. Frequency of apoptotic cells was estimated by counting the percentage of phosphatidylserine-positive/propidium iodide (PI)-negative cells using the Annexin V/PI kit (ImmunoStep, DY-634). Adherent cells were lifted with 0.25% trypsin and collected together with floating ones, centrifuged and resuspended in 190 μl of binding buffer (10 mM HEPES-NaOH pH 7.4, 140 mM NaCl, 2.5 mM $CaCl_2$) before addition of annexin V and PI. A total of 5,000 cells were analyzed in a FACScan equipped with a 488 nm argon laser using the CellQuest software (Becton-Dickinson).

Lysosomal membrane permeabilization assay. Lysosomal membrane permeabilization (LMP) was assayed with the acridine orange (AO) uptake technique.[26] Following treatments, cells were loaded for 15 min at 37 °C with 5 μg/ml AO (final concentration) in complete growth medium. Attached and floating cells were collected and resuspended in 200 μl of PBS. AO fluorescence from 10,000 cells/sample was measured by flow cytometry, as described above. Cells with lowest red

fluorescence ('pale' cells, indicating cells with a diminished number of intact lysosomes) were recorded.

Detection of plasma membrane permeabilization. Detection of plasma membrane permeabilization in cells showing LMP was accomplished with GelGreen (Biotium, 41005). Briefly, cells were treated or not with TNF/CHX and stained with LysoTracker Red as described. GelGreen was then added at a final dilution of 1:10,000 and incubated for additional 10 min at 37 °C in complete growth medium to allow a good staining of necrotic cells. When plasma membrane permeability was investigated in cells loaded with DCF-DA, 30 µg/ml of propidium iodide was added to the growth medium just before microscopic analysis. In both cases, the cultures were observed, and representative pictures captured and imaged as described above.

~~ATG7 d~~**Downregulation of MT1A, 2A and ATG7 by RNA interference.** MT1A and 2A silencing was obtained by transfecting HTC cells with 15 pmoles (50 nM final concentration) of a Mission predesigned siRNA (Sigma-Aldrich, SASI_Rn01_00065310 for MT1A and SASI_Rn01_00332519 for MT2A) with Metafectene Pro (Biontex, T040). As higher concentrations of MT-targeting siRNAs were highly toxic to these cells, for simultaneous silencing of both MT1A and 2A 10 and 5 pmoles of each siRNA were used per each well, respectively, thereby keeping the total siRNA concentration as low as 50 nM. Cells were incubated with the indicated amounts of each siRNA for 72 h; 50 µM $ZnCl_2$ was added following 48 h of transfection and left for another 24 h. Medium was then changed to either normal growth medium or to HBSS for starvation for 2 h, after which cells were exposed to TNF/CHX as described.

ATG7 silencing was achieved by targeting the rat isoform. HTC cells were transfected for 72 h in complete growth medium with 30 pmoles (100 nM final concentration) of a Mission predesigned siRNA (Sigma-Aldrich, SASI_Rn01_00050326) using MefactenePro ~~(Biontex, T040)~~. siRNA with random sequence were used as a control reaction at the same concentration and with

the same administration schedule. Then, after a change of medium, cells were treated with TNF/CHX as indicated. All siRNAs used for these experiments (MT1A, 2A and ATG7) were maintained in the medium during all treatments, namely MT induction with 50 μM $ZnCl_2$ for 24 h, starvation for 2 h in HBSS and TNF/CHX treatment for 6 h.

Western blot analysis of MT and SQSTM1/p62. MT detection was performed essentially as described.[65] Briefly, control and $ZnCl_2$-exposed cells were scraped from the growth flasks, washed with PBS and centrifuged at 100 RCF for 10 min at 4 °C. Pellets were resuspended with 10 mM TRIS-Cl, pH 7.0, 5 mM EDTA containing 1 mM PMSF and immediately frozen at -80 °C to obtain complete cell rupture. Defrosted samples were then centrifuged at 20,000 RCF for 45 min at 4 °C; 30 μg of each sample was fractionated on a 12% NuPAGE gel (Invitrogen, NP0341), transferred and fixed to nitrocellulose according to Mizzen *et al.*[66] An overnight incubation with a primary mouse monoclonal antibody against metallothionein-I and -II (1:1,000, Zymed Laboratories Inc., 18-0133) was followed by 4 h of incubation with an alkaline phosphatase-conjugated secondary antibody (1:1,000, Sigma-Aldrich, A4312) and a chromogenic substrate (BCIP/NBT, Sigma-Aldrich, 72091) for visualization of the bands.

For analysis of SQSTM1 degradation, aliquots of 20 μg of total lysates from controls and cells treated with 100 μM E-64-d plus 10 μM leupeptin were fractionated on a 12% acrylamide gel and transferred to nitrocellulose. Membranes were then probed with an anti-SQSTM1 antibody (Sigma-Aldrich, P0067) for 60 min at 4 °C. As a control for loading, membranes were subsequently probed with a mouse monoclonal anti-~~β~~ β-actin antibody (clone AC-15; 1:4,000, Sigma-Aldrich, A5441), and washed with 0.05% TBS-Tween. After incubation with an anti-IgG antibody (1:10,000, Bio-Rad Laboratories, 172-1011 or 170-6515) chemiluminescent detection was performed with the ImmunoCruz Western Blotting Luminol Reagent (Santa Cruz Biotechnology, sc-2048).

Statistical analysis. Data represent means ± SD from at least three independent experiments, each assayed in triplicate. Differences between groups were analyzed either by one-way ANOVA followed by Student-Newman-Keuls post-test or by the Student's t test using Instat (Ver. 3.01, GraphPad).

Disclosure of potential conflicts of interest

No potential conflicts of interest were disclosed.

Acknowledgments

This work was supported by grants from Ministero dell'Università e della Ricerca and Università degli Studi di Torino. We are grateful to Prof. Tamotsu Yoshimori, Graduate School of Medicine, Osaka, JPN, Prof. Steven Johnson, Oregon Health and Science University, Portland, OR, USA and Prof. David Sabatini, Department of Biology, Massachusetts Institute of Technology, Cambridge, USA, for having kindly provided us with the constructs encoding for the tfLC3, GFP-MT2A and for the mCherry-LIC (6B) backbone, respectively; to Prof. John W. Eaton, University of Louisville, KY, USA, for his critical reading of the manuscript and valuable suggestions and to Prof. Ana Maria Cuervo, Albert Einstein College of Medicine, NY, USA, for valuable suggestions on ATG protein silencing.

References

1. Bradley JR. TNF-mediated inflammatory disease. J Pathol 2008; 214:149-60.
2. Schwabe RF, Brenner DA. Mechanisms of liver injury. I. TNF-alpha-induced liver injury: role of IKK, JNK, and ROS pathways. Am J Physiol Gastrointest Liver Physiol 2006; 290:G583-G589.
3. Grell M, Douni E, Wajant H, Löhden M, Clauss M, Maxeiner B, Georgopoulos S, Lesslauer W, Kollias G, Pfizenmaier K, et al. The transmembrane form of tumor necrosis factor is the prime activating ligand of the 80 kDa tumor necrosis factor receptor. Cell 1995; 83:793-802.
4. Rodriguez M, Cabal-Hierro L, Carcedo MT, Iglesias JM, Artime N, Darnay BG, Lazo PS. NF-kB signal triggering and termination by tumor necrosis factor receptor 2. J Biol Chem 2011; 286:22814-24.
5. Tartaglia LA, Pennica D, Goeddel DV. Ligand passing: the 75-kDa tumor necrosis factor (TNF) receptor recruits TNF for signaling by the 55-kDa TNF receptor. J Biol Chem 1993; 268:18542-8.
6. Scaffidi C, Fulda S, Srinivasan A, Friesen C, Li F, Tomaselli KJ, Debatin KM, Krammer PH, Peter ME. Two CD95 (APO-1/Fas) signaling pathways. EMBO J 1998; 17:1675-87.
7. Leist M, Jäättelä M. Four deaths and a funeral: from caspases to alternative mechanisms. Nat Rev Mol Cell Biol 2001; 2:589-98.
8. Lockshin RA, Zakeri Z. Caspase-independent cell deaths. Curr Opin Cell Biol 2002; 14:727-33.
9. Alessenko AV, Boikov PY, Filippova GN, Khrenov AV, Loginov AS, Makarieva ED. Mechanisms of cycloheximide-induced apoptosis in liver cells. FEBS Lett 1997; 416:113-6.
10. Duriez PJ, Wong F, Dorovini-Zis K, Shahidi R, Karsan A. A1 functions at the mitochondria to delay endothelial apoptosis in response to tumor necrosis factor. J Biol Chem 2000; 275:18099-107.

11. Lüschen S, Ussat S, Scherer G, Kabelitz D, Adam-Klages S. Sensitization to death receptor cytotoxicity by inhibition of fas-associated death domain protein (FADD)/caspase signaling. Requirement of cell cycle progression. J Biol Chem 2000; 275:24670-8.
12. Warren S, Torti SV, Torti FM. The role of iron in the cytotoxicity of tumor necrosis factor. Lymphokine Cytokine Res 1993; 12:75-80.
13. Jones BE, Lo CR, Liu H, Srinivasan A, Streetz K, Valentino KL, Czaja MJ. Hepatocytes sensitized to tumor necrosis factor-alpha cytotoxicity undergo apoptosis through caspase-dependent and caspase-independent pathways. J Biol Chem 2000; 275:705-12.
14. Monney L, Olivier R, Otter I, Jansen B, Poirier GG, Borner C. Role of an acidic compartment in tumor-necrosis-factor-alpha-induced production of ceramide, activation of caspase-3 and apoptosis. Eur J Biochem 1998; 251:295-303.
15. Werneburg N, Guicciardi ME, Yin XM, Gores GJ. TNF-alpha-mediated lysosomal permeabilization is FAN and caspase 8/Bid dependent. Am J Physiol Gastrointest Liver Physiol 2004; 287:G436-G443.
16. Kroemer G, Jäättelä M. Lysosomes and autophagy in cell death control. Nat Rev Cancer 2005; 5:886-97.
17. Terman A, Kurz T. Lysosomal iron, iron chelation and cell death. Antioxid Redox Signal 2013; 18:888-98.
18. Terman A, Kurz T, Gustafsson B, Brunk UT. Lysosomal labilization. IUBMB Life 2006; 58:531-9.
19. Kurz T, Gustafsson B, Brunk UT. Cell sensitivity to oxidative stress is influenced by ferritin autophagy. Free Radic Biol Med 2011; 50:1647-58.
20. Kurz T, Brunk UT. Autophagy of HSP70 and chelation of lysosomal iron in a non-redox-active form. Autophagy 2009; 5:93-5.
21. Gyrd-Hansen M, Nylandsted J, Jäättelä M. Heat shock protein 70 promotes cancer cell viability by safeguarding lysosomal integrity. Cell Cycle 2004; 3:1484-5.

22. Autelli R, Crepaldi S, De Stefanis D, Parola M, Bonelli G, Baccino FM. Intracellular free iron and acidic pathways mediate TNF-induced death of rat hepatoma cells. Apoptosis 2005; 10:777-86.

23. Autelli R, Ullio C, Prigione E, Crepaldi S, Schiavone N, Brunk UT, Capaccioli S, Baccino FM, Bonelli G. Divergent pathways for TNF and C(2)-ceramide toxicity in HTC hepatoma cells. Biochim Biophys Acta 2009; 1793:1182-90.

24. Ullio C, Casas J, Brunk UT, Sala G, Fabriàs G, Ghidoni R, Bonelli G, Baccino FM, Autelli R. Sphingosine mediates TNFalpha-induced lysosomal membrane permeabilization and ensuing programmed cell death in hepatoma cells. J Lipid Res 2012; 53:1134-43.

25. Yu Z, Persson HL, Eaton JW, Brunk UT. Intralysosomal iron: a major determinant of oxidant-induced cell death. Free Radic Biol Med 2003; 34:1243-52.

26. Zhao M, Eaton JW, Brunk UT. Protection against oxidant-mediated lysosomal rupture: a new anti-apoptotic activity of Bcl-2? FEBS Lett 2000; 485:104-8.

27. Karlsson M, Kurz T, Brunk UT, Nilsson SE, Frennesson CI. What does the commonly used DCF test for oxidative stress really show? Biochem J 2010; 428:183-90.

28. Øverbye A, Sætre F, Hagen LK, Johansen HT, Seglen PO. Autophagic activity measured in whole rat hepatocytes as the accumulation of a novel BHMT fragment (p10), generated in amphisomes by the asparaginyl proteinase, legumain. Autophagy 2011; 7:1011-27.

29. Baird SK, Kurz T, Brunk UT. Metallothionein protects against oxidative stress-induced lysosomal destabilization. Biochem J 2006; 394:275-83.

30. Andrews GK. Regulation of metallothionein gene expression by oxidative stress and metal ions. Biochem Pharmacol 2000; 59:95-104.

31. Koyama-Honda I, Itakura E, Fujiwara TK, Mizushima N. Temporal analysis of recruitment of mammalian ATG proteins to the autophagosome formation site. Autophagy 2013; 9:1491-9.

32. Eng KE, Panas MD, Karlsson Hedestam GB, McInerney GM. A novel quantitative flow cytometry-based assay for autophagy. Autophagy 2010; 6:634-41.
33. Shishodia S, Aggarwal BB. Nuclear factor-kappaB activation: a question of life or death. J Biochem Mol Biol 2002; 35:28-40.
34. Vandenabeele P, Galluzzi L, Vanden BT, Kroemer G. Molecular mechanisms of necroptosis: an ordered cellular explosion. Nat Rev Mol Cell Biol 2010; 11:700-14.
35. Chipuk JE, Green DR. Do inducers of apoptosis trigger caspase-independent cell death? Nat Rev Mol Cell Biol 2005; 6:268-75.
36. Wilson CA, Browning JL. Death of HT29 adenocarcinoma cells induced by TNF family receptor activation is caspase-independent and displays features of both apoptosis and necrosis. Cell Death Differ 2002; 9:1321-33.
37. Dada LA, Sznajder JI. Mitochondrial Ca(2)+ and ROS take center stage to orchestrate TNF-alpha-mediated inflammatory responses. J Clin Invest 2011; 121:1683-5.
38. Kim JJ, Lee SB, Park JK, Yoo YD. TNF-alpha-induced ROS production triggering apoptosis is directly linked to Romo1 and Bcl-X(L). Cell Death Differ 2010; 17:1420-34.
39. Sakon S, Xue X, Takekawa M, Sasazuki T, Okazaki T, Kojima Y, Piao JH, Yagita H, Okumura K, Doi T, et al. NF-kappaB inhibits TNF-induced accumulation of ROS that mediate prolonged MAPK activation and necrotic cell death. EMBO J 2003; 22:3898-909.
40. Lloyd JB, Cable H, Rice-Evans C. Evidence that desferrioxamine cannot enter cells by passive diffusion. Biochem Pharmacol 1991; 41:1361-3.
41. Kurz T, Eaton JW, Brunk UT. The role of lysosomes in iron metabolism and recycling. Int J Biochem Cell Biol 2011; 43:1686-97.
42. Levi S, Rovida E. The role of iron in mitochondrial function. Biochim Biophys Acta 2009; 1790:629-36.
43. Brunk UT, Neuzil J, Eaton JW. Lysosomal involvement in apoptosis. Redox Rep 2001; 6:91-7.

44. Persson HL, Nilsson KJ, Brunk UT. Novel cellular defenses against iron and oxidation: ferritin and autophagocytosis preserve lysosomal stability in airway epithelium. Redox Rep 2001; 6:57-63.

45. Kim YS, Morgan MJ, Choksi S, Liu ZG. TNF-induced activation of the Nox1 NADPH oxidase and its role in the induction of necrotic cell death. Mol Cell 2007; 26:675-87.

46. Basuroy S, Bhattacharya S, Leffler CW, Parfenova H. Nox4 NADPH oxidase mediates oxidative stress and apoptosis caused by TNF-alpha in cerebral vascular endothelial cells. Am J Physiol Cell Physiol 2009; 296:C422-C432.

47. Chen CS. Phorbol ester induces elevated oxidative activity and alkalization in a subset of lysosomes. BMC Cell Biol 2002; 3:21-32.

48. Droga-Mazovec G, Bojic L, Petelin A, Ivanova S, Romih R, Repnik U, Salvesen GS, Stoka V, Turk V, Turk B. Cysteine cathepsins trigger caspase-dependent cell death through cleavage of bid and antiapoptotic Bcl-2 homologues. J Biol Chem 2008; 283:19140-50.

49. Nilsson E, Ghassemifar R, Brunk UT. Lysosomal heterogeneity between and within cells with respect to resistance against oxidative stress. Histochem J 1997; 29:857-65.

50. Czaja MJ. Two types of autophagy are better than one during hepatocyte oxidative stress. Autophagy 2011; 7:96-7.

51. Lv XC, Zhou HY. Resveratrol protects H9c2 embryonic rat heart derived cells from oxidative stress by inducing autophagy: role of p38 mitogen-activated protein kinase. Can J Physiol Pharmacol 2012; 90:655-62.

52. Marino ML, Fais S, Djavaheri-Mergny M, Villa A, Meschini S, Lozupone F, Venturi G, Della Mina P, Pattingre S, Rivoltini L, et al. Proton pump inhibition induces autophagy as a survival mechanism following oxidative stress in human melanoma cells. Cell Death Dis 2010; 1:e87. doi: 10.1038/cddis.2010.67.:e87.

53. Chiaverini N, De Ley M. Protective effect of metallothionein on oxidative stress-induced DNA damage. Free Radic Res 2010; 44:605-13.

54. Lu H, Hunt DM, Ganti R, Davis A, Dutt K, Alam J, Hunt RC. Metallothionein protects retinal pigment epithelial cells against apoptosis and oxidative stress. Exp Eye Res 2002; 74:83-92.

55. Weng CJ, Chen MJ, Yeh CT, Yen GC. Hepatoprotection of quercetin against oxidative stress by induction of metallothionein expression through activating MAPK and PI3K pathways and enhancing Nrf2 DNA-binding activity. N Biotechnol 2011; 28:767-77.

56. You HJ, Lee KJ, Jeong HG. Overexpression of human metallothionein-III prevents hydrogen peroxide-induced oxidative stress in human fibroblasts. FEBS Lett 2002; 521:175-9.

57. Lee SJ, Koh JY. Roles of zinc and metallothionein-3 in oxidative stress-induced lysosomal dysfunction, cell death, and autophagy in neurons and astrocytes. Mol Brain 2010; 3:30-8.

58. Pedersen MO, Larsen A, Stoltenberg M, Penkowa M. The role of metallothionein in oncogenesis and cancer prognosis. Prog Histochem Cytochem 2009; 44:29-64.

59. Choudhuri S, McKim JM, Jr., Klaassen CD. Role of hepatic lysosomes in the degradation of metallothionein. Toxicol Appl Pharmacol 1992; 115:64-71.

60. Klaassen CD, Choudhuri S, McKim JM, Jr., Lehman-McKeeman LD, Kershaw WC. In vitro and in vivo studies on the degradation of metallothionein. Environ Health Perspect 1994; 102 Suppl 3:141-6.

61. Kimura S, Noda T, Yoshimori T. Dissection of the autophagosome maturation process by a novel reporter protein, tandem fluorescent-tagged LC3. Autophagy 2007; 3:452-60.

62. Porter K, Nallathambi J, Lin Y, Liton PB. Lysosomal basification and decreased autophagic flux in oxidatively stressed trabecular meshwork cells: implications for glaucoma pathogenesis. Autophagy 2013; 9:581-94.

63. Chu CT, Plowey ED, Dagda RK, Hickey RW, Cherra SJ, III, Clark RS. Autophagy in neurite injury and neurodegeneration: in vitro and in vivo models. Methods Enzymol 2009; 453:217-49.

64. Bolte S, Cordelieres FP. A guided tour into subcellular colocalization analysis in light microscopy. J Microsc 2006; 224:213-32.

65. Urani C, Melchioretto P, Gribaldo L. Regulation of metallothioneins and ZnT-1 transporter expression in human hepatoma cells HepG2 exposed to zinc and cadmium. Toxicol In Vitro 2010; 24:370-4.

66. Mizzen CA, Cartel NJ, Yu WH, Fraser PE, McLachlan DR. Sensitive detection of metallothioneins-1, -2 and -3 in tissue homogenates by immunoblotting: a method for enhanced membrane transfer and retention. J Biochem Biophys Methods 1996; 32:77-83.

FIGURE LEGENDS

Figure 1. Iron affects TNF/CHX toxicity in HTC cells. (**A**) Cells were exposed for 2 h to a precipitate of hydrated iron-phosphate, which spontaneously forms when $FeCl_3$ is added to the medium, and subsequently treated with 20 ng/ml TNF plus 10 μg/ml CHX for another 6 h. Cells were then loaded for 15 min with acridine orange (AO) at a final concentration of 5 μg/ml in complete growth medium and analyzed by flow cytometry. 10,000 cells were run each time in a FACScan flow cytometer; data were collected and analyzed with the CellQuest software. 'Pale' cells represent the population with the lowest red fluorescence (as illustrated in Fig. 3D) when exposed to green light, due to a reduced number of normal lysosomes. (**B**) Cells were incubated with either 1 μM apoferritin (ApoF) for 4 h or 250 μM deferiprone (Dfp) for 18 h before being exposed to TNF/CHX for 6 h. At the end of treatment, the number of annexin V-positive/PI-negative cells (black bars) and of 'pale' cells (light gray bars) was measured on 5,000 and 10,000 cells per sample as described above. (**C**) Cells were treated with TNF/CHX as in (**A**), sequentially stained with LysoTracker Red and GelGreen as indicated in Materials and Methods and observed under a fluorescence microscope. The frame in the left panel (phase contrast) was electronically magnified and the red and green channels reproduced, either separately (middle two panels) or overlaid in the rightmost panel. Arrowheads indicate moderately shrunk cells undergoing initial LMP, but still retaining plasma membrane selective permeability, as is implied by their impermeability to GelGreen. The arrow points to a strongly condensed cell with fully permeabilized lysosomes, taking up the GelGreen dye, suggestive of a late phase of death ("late apoptotic" or "secondary necrotic" cell).

Data represent the means ± SD of at least three independent experiments. *, **, ***: $p < 0.05$, $p < 0.01$ and $p < 0.001$, respectively, *vs* TNF/CHX (ANOVA).

Figure 2. TNF/CHX exposure triggers redox reactions that involve the lysosomal compartment. (**A**) Cells were left untreated (top panels), or treated with TNF/CHX as in Fig. 1 (bottom panels).

Cultures were then exposed for 30 min to 10 µM dichlorofluorescein diacetate (DCF-DA) in medium without phenol red, rinsed with fresh growth medium and observed under an inverted fluorescence microscope. ~~Occasional c~~Cells with evident TNF/CHX-related morphological alterations displayed a lysosomal-type punctate intense fluorescence (arrowheads), while other cells, in which morphological changes were not yet so established displayed less intense green fluorescence (arrows), suggesting the process to still be in a very early phase. (**B**) Cells were treated with TNF/CHX and sequentially loaded with 10 µM DCF-DA as in (**A**) and, just before observation, stained with 30 µg/ml of PI. The green fluorescent cells (showing "granular" DCF-DA-positivity) do not take up PI, indicating that redox reactions occur in an early phase of the death process. (**C**) Cells were treated with TNF/CHX as in (**A**) and sequentially loaded with 10 µM DCF-DA and 25 nM LysoTracker Red DND-99 as described in Materials and Methods. Controls (upper panels) and cells treated with TNF/CHX (lower panels) were observed and photographed as in (**A**). Arrows indicate lysosomes that are not stained by DCF. The pictures shown in (**A-C**) are representative of three different experiments for each condition.

Figure 3. Induction of autophagy and inhibition of lysosomal proteolysis protect from TNF/CHX-induced death. (**A**) Cells were transfected with ptfLC3, starved in amino acid-free medium (HBSS containing glucose) for 2 h and examined with a confocal microscope (left panel) for quantification (histograms) of yellow and red fluorescent dots/cell representing autophagosomes and autolysosomes, respectively. Amino acid deprivation increases number and size of both autophagosomes and autolysosomes, suggestive of enhanced autophagic flux. The number of cells examined for autophagosomes/autolysosomes quantification is indicated in each bar. (**B**) The kinetics of SQSTM1 degradation was assayed by western blotting (left panel, representative of three independent experiments) under both control conditions and following starvation for 2 h in HBSS/glucose, in the absence or presence of 100 µM E-64-d and 10 µM leupeptin (E64d/Leu, for the full period of starvation), to inhibit lysosomal proteolysis. Normalization was performed against

the level of β-actin of each sample. The relative amount of SQSTM1 was expressed *vs* that of time 0 for each condition (histograms, right panel). (**C**) Cells starved as above for 2 h were exposed to TNF/CHX for 6 h in the absence or presence of 20 mM NH_4Cl, added during the last 60 min of starvation, or of 100 μM E-64-d and 10 μM leupeptin for the whole period of starvation. The percentage of apoptotic-like cells (phosphatidylserine-positive and PI-negative) was then quantified by flow cytometry (5,000 cells were analyzed for each sample). Only occasional necrotic (PI positive) cells were found. (**D**) Cells were exposed for 6 h to TNF/CHX following 2 h of starvation (upper panel) or 1 h of incubation with NH_4Cl (middle panel), loaded with AO and analyzed by flow cytometry on 10,000 cells. The fluorescence intensity peak of control cells was set approximately at channel 10^3 and retained for all measurements. Arrowheads indicate the peaks of the lowest red-fluorescent population (here referred to as maximally 'pale' cells) resulting from cells with the most reduced number of intact lysosomes due to LMP. Histograms (lower panel) show the percentage of these pale cells from electronic gating and counting.

Yellow and red bars in the right panel of **Fig. 3A** indicate the number (means ± SD) of autophagosomes and autolysosomes/cell, respectively; the number of cells analyzed for each condition is indicated inside relevant bars; *: $p < 0.002$ (Student's t test). The asterisk in (**B**) indicates a non-specific band. For (**C**) and (**D**) data and significance are as in Fig. 1. **, ***: $p < 0.01$ and $p < 0.001$ *vs* TNF/CHX.

Figure 4. Effect of MT upregulation and ensuing autophagy on TNF/CHX toxicity. (**A**) Cells were exposed to 50 μM $ZnCl_2$ for 24 h. Changes of metallothionein 1A (MT1A) and 2A (MT2A) mRNA levels were measured by real time RT-PCR and presented as relative amounts with respect to untreated cells. (**B**) Cells were exposed for 24 h to the indicated concentrations of $ZnCl_2$ and levels of MT1A mRNA were analyzed by real time RT-PCR and normalized to GAPDH mRNA (upper panel). Equal amounts of proteins from each sample were separated on a 12% denaturing PAGE and transferred to a nitrocellulose membrane for probing with an anti-MT antibody (middle panel).

Loading was assayed by reprobing the membrane with an anti-β-actin antibody (lower panel). (**C**) Cells were treated with $ZnCl_2$ as in (**A**) and starved for different period of times to measure degradation rate of SQSTM1 in the absence or presence of E64d/Leu as in Fig. 3B (representative of three independent experiments). The change in relative amounts of protein at various time points (histograms, right panel) indicates that treatment with 50 μM $ZnCl_2$ to upregulate MTs does not substantially affect autophagic flux. To demonstrate autophagic sequestration of MT (**D-E**) cells were transfected with the plasmids encoding both human MT2A-mCherry and pEGFP-C1-LC3, either left untreated (**D**) or subsequently starved (**E**) in the presence of the various lysosomal inhibitors as indicated. Colocalization is not observed in non-starved cells (**D**), although it is in starved cells, where it is indicated by yellow puncta (**E**, arrowheads). To show lysosomal delivery of autophagocytosed MT (**F-G**), cells were transfected with both hMT2A-GFP and the lysosomal marker LAMP1-mRFP. In unstarved cells (**F**) red and green fluorescence do not overlap. Upon starvation in the presence of various inhibitors of lysosomal degradation (**G**) several enlarged red-labeled, ring-shaped organelles representing lysosomes, which apparently have engulfed some intensely green-fluorescent material, indicate lysosomes containing non-degraded MT2A-GFP (arrows). (**H**) Cells were treated with TNF/CHX following exposure to $ZnCl_2$ for 24 h and ensuing starvation for 2 h. The percentage of apoptotic cells was determined by flow cytometry as in Fig. 1B. (**I**) Maximally pale cells (arrowhead) were detected and quantified as in Fig. 3C. Note almost complete protection in MT-upregulated, starved cells. Numerical data from three independent experiments are presented in the below histograms. For (**H**) and (**I**) 5,000 and 10,000 cells were analyzed for each sample, respectively. The asterisk in (**C**) indicates a non-specific band. Data and statistical significance are as in Fig. 1; §§, §§§; $p < 0.01$ and $p < 0.001$ *vs* controls; ***: $p < 0.001$ *vs* TNF/CHX.

Figure 5. ATG7 silencing abrogates protection from TNF/CHX by MT upregulation and starvation-induced enhanced autophagy. (**A**) Cells were incubated for 72 h with 100 nM siRNA specific for rat

ATG7 and treated with 50 μM $ZnCl_2$ during the last 24 h. ATG7, MT1A and 2A mRNAs were quantified by real time RT-PCR and expressed as relative amounts *vs* cells transfected with non-specific siRNAs. (**B**) The effect of ATG7 silencing on starvation-induced autophagic flux was assayed by transfecting mock- and ATG7-silenced cells with the ptfLC3 construct as described in the legend to Fig. 3A. Quantification of autophagosomes and autolysosomes was performed on single-cell images obtained by confocal microscopy. (**C**) MT was induced with 50 μM $ZnCl_2$ in both control- and ATG7-silenced cells, starved as indicated and exposed to TNF/CHX for another 6 h. Adherent and floating cells were pooled and analyzed by FACS with the annexin V/PI technique. At least 5,000 cells were assayed for each condition. (**D**) Mock- and ATG7-silenced cells were treated with various concentrations of $FeCl_3$, starved and treated with TNF/CHX as described in Fig. 1A. The percentage of pale cells was quantified by FACS as in Fig. 1A.

For panels **A**, **C** and **D** data and statistical analysis of differences are as in Fig. 1; §, §§§: $p < 0.05$ and $p < 0.001$ *vs* control-silenced cells; **, ***: $p < 0.01$ and $p < 0.001$ *vs* TNF/CHX. For panel **B**, yellow and red bars indicate the number (mean ± SD) of autophagosomes and autolysosomes/cell, respectively. The number of cells analyzed for each condition is indicated inside relevant bars; *: $p < 0.005$ (Student's t test).

siControl, siATG7: non-specific and ATG7-specific siRNAs, respectively.

Figure 6. MT silencing abrogates protection from TNF/CHX conferred by MT upregulation. (**A**) Cells were incubated for 72 h with 50 nM siRNAs targeting rat MT1A and 2A (dark and light grey bars, respectively) and treated with 50 μM $ZnCl_2$ during the last 24 h of siRNA treatment. MT1A and 2A mRNAs were quantified by real time RT-PCR and expressed as relative amounts *vs* cells transfected with non-specific siRNAs. The effect of mock and combined MT1A/2A silencing (black and white bars, respectively, **B**), as well as of MT1A alone (**C**) or MT2A alone (**D**) knockdown on protection by $ZnCl_2$ and starvation-induced autophagy against TNF/CHX toxicity was assayed in cells silenced as indicated, treated with $ZnCl_2$ to upregulate MT, starved for 2 h in HBSS/glucose

and eventually exposed to TNF/CHX. Adherent and floating cells were pooled and analyzed by FACS with the annexin V/PI technique. At least 5,000 cells were assayed for each condition. Data and statistical significance are as in Fig. 1; *, **, ***: $p < 0.05$, $p < 0.01$ and $p < 0.001$ *vs* TNF/CHX-treated cells (panels B, **C** and **D**) or mock-silenced cells treated with $ZnCl_2$ (panels **A)**. §§; $p < 0.01$ *vs* cells silenced with siRNAs against both MT1A and 2A and treated with TNF/CHX (panel **B**).

siControl, siMT1A and siMT2A: non-specific, MT1A- and MT2A-specific siRNAs, respectively.